Results in Engineering 25 (2025) 103951

Contents lists available at ScienceDirect

Results in Engineering

journal homepage: www.sciencedirect.com/journal/results-in-engineering

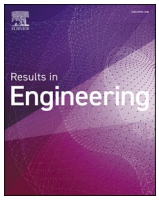

A robust automatic generation control system based on hybrid Aquila Optimizer-Sine Cosine Algorithm

Sadeq D. Al-Majidi [a,*], Al_hussein M. Alturfi [a], Mohammed Kh. Al-Nussairi [a], Rasha Abed Hussein [b], Rohit Salgotra [c], Maysam F. Abbod [d]

[a] Department of Electrical Engineering, College of Engineering, University of Misan, Amarah 62001, Iraq
[b] Department Of Dentistry, Al-Manara College for Medical Sciences, Maysan, Iraq
[c] Faculty of Physics and Applied Computer Science, AGH University of Krakow, Poland
[d] Department of Electronic and Electrical Engineering, College of Engineering, Brunel University London, Uxbridge UB8 3PH, United Kingdom

ARTICLE INFO

Keywords:
Automatic generation controller
Proportional-integral-derivative
Aquila optimizer
Sine cosine algorithm and power system network

ABSTRACT

The fluctuating frequency in a power grid is the major stability challenge duo to the unpredictable power demand of costumers during the time. To address this issue, automatic generation controller (AGC) is employed. The AGC based on a proportional integral derivative (PID) approach is popularly utilised owing to its soft implementation and lower expenditure. However, it ripples to handle the standard frequency of a multi-area power grid that occurs in a competitive load-demand case, because of the high sensitivity of its uncertain parameters. In this paper, a Hybrid Aquila Optimizer-Sine Cosine algorithm (HSCAO) is designed for addressing the sensitivity of the PID-AGC parameters specifically for the multi-area power system network. The suggested algorithm is assessed based on CEC-2019, and classical benchmark issues with various dimensions to validate its performance and address the better fits of the algorithm parameters adequately. Also, a statistical analysis technique is conducted using Wilcoxon's test and Friedman test to demonstrate the supervise performance of the HSCAO optimisation regarding to other relative optimal algorithms. A two-area power system network is simulated using MATLAB environment to implement the proposed AGC system. The outcomes prove that the optimal PID-AGC method based on HSCAO technique demonstrates its ability to address the simple and complex fluctuations of load demands quickly. Also, it is the most robust to supervise the frequency response under fault condition test, resulting in, achieving the lowest ITAE index of 5.2s compared to the conventional fuzzy logic control-AGC and the conventional PID-AGC of 10.9s and 17.4s respectively.

List of notations

Variables	Notations
Ω(s)	Accelerating generator
H	Inertia of generator
ΔPm	Historical change in mechanical power
Δpe	Historical change in electrical power
ΔPL	Resister's load-demand
Δω	Motor's miss
Pref	Generating power
R	Regulator- speed
Pg	Electrical power production
τg	Time-constant speed of the turbine
ΔPv	Change in steam size of the turbine
e1 and e2	AC-frequency errors of the Areas 1& 2.
Δf	Frequency deviation in power system network
α	The synchronizing coefficient for Tie Line
Kd	Derivative gain of PID
Ki	Integral gain of PID
Kp	Proportional gain of PID
Y_i^t and Y_i^{t+1}	i^{th} location of the current solution during iteration 't' and the next iteration 't+1', respectively
r_1, r_2, r_3 and r_4	Randomly generated integers of SCA algorithm
P_i^t	Most optimal solution at the i^{th} position in the collection of solutions
T	Highest iteration
t	Present iteration
Y_{best}	Optimal position

* Corresponding author.
E-mail address: sadeqalmajidi@uomisan.edu.iq (S.D. Al-Majidi).

https://doi.org/10.1016/j.rineng.2025.103951
Received 3 November 2024; Received in revised form 7 December 2024; Accepted 3 January 2025
Available online 11 January 2025

Dim	Dimension size
N	Population size
LF(D)	Levy flight distribution function
u and υ	Values are generated at random from 0 to 1
A	Fixed value of HSCAO algorithm that is established at 2.
β	Fixed value of HSCAO algorithm that is established at 1.5.
r_5	Number of search cycles ranging from 1 to 20
γ and δ	Parameters for exploitation adjustment are set at 0.1
Lb & Ub	Lower limit & upper bound.
QF(t)	Quality measure of the search approach
G_1 & G_2	Aquila's mobility factors
ΔP_{tie}	Tie Line power deviation
u_1 & u_2	Control inputs in Areas 1& 2.
ΔP_{g1} & ΔP_{g2}	The output power deviations at governor
ΔP_{t1} & ΔP_{t2}	The output deviations at Turbine
$\Delta P_1 = D_1$	The load disturbances in Areas 1
$\Delta P_2 = D_2$	The load disturbances in Areas 2.
K_1&K_2	The constants of Areas 1&2.
τ_{P1}&τ_{P2}	The time constants of Areas 1& 2.
ACE	The processing error of power system
B_1 & B_2	The Tie-Line frequency bias at Areas 1&2.

1. Introduction

Regrading to the multi-generation units and the electrical fluctuating demands on the modern power grid, the frequency response of a power system network is changing dramatically. This is causing the instability of the power generation and the sensitivity of a frequency level specifically for the muti-area power network. Hence, automatic generation controller (AGC) is utilised to retrieve the frequency response and regulate the power delivery by adjusting the accelerated governor speed of the generator units based on considering the size of fuel, resulting in, matching the power delivery with the power demand [1]. Consequently, the frequency level restores to the standard value for the power system. In the first design prototype of AGC, the researchers proposed the flywheel controller for the AC-machine of generation to dampen the frequency oscillation. However, it is not addressing the oscillation suppression of the system when the loads are changing rapidly due to the complex functionality of the AGC [2]. To design the accurate AGC in the significant uncertainty of the multi-area power network, a robust control system is required. This is because the robust control system exhibits lower sensitivities for the change of highly parameter variations.

Recently, a proportional-integral-derivative (PID) has been added to AGC system as a compensator because of its simpler accomplishment and lower expenditure when compared with the classical control system [3]. However, it faces the high frequency sensitivity under a competitive load-demand specifically for the multi-area power grid owing to its constant parameters, resulting in, poor dynamic performance. Hence, several techniques had been used to adjust the parameters of the PID controller. Among them, the authors in [4] proposed a novel PID controller based on fuzzy logic controller (FLC) for the AGC system of a two-area grid-connected system. The FLC is employed to address the fixed elements of the PID controller adequately using the membership function tools. The results of this proposal show that it has ability to demonstrate the oscillations in the frequency response for various power generation tests. Next, the authors in [5] designed a hybrid FLC-PID controller with filter-fractional order integral for a two-area AGC system. Firstly, the FLC technique is used to enhance the input of PID controller, then, the filter-fractional order integral is demonstrated the output of PID controller. The results of this study prove that the proposed method address the various load disturbances when it is compared with different conventional methods. Similarity, the scholars in [6] employed the PID controller based on the type-2 of the FLC method for the AGC system of a two-area grid network. The tuning parameters of the FLC-AGC system is addressed in this work using a novel adaptive symbiotic organism search technique. The outcomes of this work show that it returns the zero-point of frequency level with less undershoot, overshoot and settling time. Although, those previous studies have been provided the optimal AGC system under various states. However, they did not discuss the ITAE performance index for the power system network under an unbalance disturbance case. Further, the studies are not cover all condition states.

In advanced step, the scholars in [7] used a developed algorithm such as sine-cosine algorithm to regulate the memberships of the FLC technique that is utilised in PID parameters. Then, this controller method is applied on the AGC controller of a multi-area power system network under different tests. The findings of this research prove that the proposed method is the highest robust to address the load disturbance tests for diverse cases. Consequently, the scholar in [8] also used a grey wolf technique which is classified as advanced algorithm to optimise the control gain of PID-AGC controller for three-area power network. Then, the FLC technique is implemented to improve the PID elements. The results of this research demonstrate that the proposed method is well supervisor to restore the frequency level of the three-area of the power grid under various simulation tests. In other side, the authors in [9] optimised a FLC-PID controller based on dragonfly algorithm for AGC system. Hence, the scaling factors of this AGC design is proposed based on the memberships of the FLC, resulting in, addressing the gains of the PID controller. The outcomes of this work prove that this proposal restores the frequency system of simulation test under the linearity and non-linearity operation works.

In the same year, the authors in [10] presented an optimal hybrid FLC-PID controller based on modified sine-cosine algorithm for two-area of the AGC system with four generation units. This modified algorithm is employed to adjust the elements of the FLC-PID controller based on two-steps. As results, the standard frequency state of the power grid test is addressed in a lower transient time with less rising undershoot and overshoot. While, the researchers in [11] designed the AGC system for multi-area power network based on interval type-2 FLC-PID technique to address the huge action of frequency diversion. Then, a deep Q-network algorithm is used to adjust the function design of the FLC under various operating conditions. The finding results of this work prove that it is improving the system performances of the AGC to carry out the frequency response level at steady state error with the short time. Alternatively, a novel fractional order integral-tilt-derivative controller for a multi-area AGC system was proposed by the authors in [12]. The AGC system's settings are then optimized using a meta-heuristic technique based on different blocks. This proposed method proves that it is more robust to address the various of power parameters until 50 % of input error signals. Lastly, the authors in [13] used an arithmetic optimized African vulture algorithm to optimise the proposed FLC-PID controller for AGC system. A hybrid deregulating power system for classical and renewable energy resources are simulated to assess the vestige of this proposal. The outcomes show that the proposed method is addressed the performance of the AGC by enhance its fitness up to 40 %. Recently, the authors in [14] developed a novel algorithm based on Aquila Optimizer to tune the parameters of the PID-AGC for a hybrid power system network. Then, it is compared with the popular optimisation algorithm such as particle swarm optimisation and whale optimization algorithm under a deregulated case. Hence, the results prove that it validates to address the stability of the hybrid power system at this type of the fault case. In last years, the optimal parameters of PID-AGC controller based on the neural network technique is used such as in [15]. This type of system shows a higher performance to avoid the load disturbances when it is applied on multiarea power grid. However, it requires priory data to train it on unpredictive cases.

As noticed that, the provirus studies show the efficiently of the AGC system based on the optimised PID controller using advanced optimisation techniques, however, they presented a complex prototype of the control system regarding to the hybrid controller stages. In addition, the processing optimisation time is not address which is considered the most important factor in the transiting case of the frequency response. Hence,

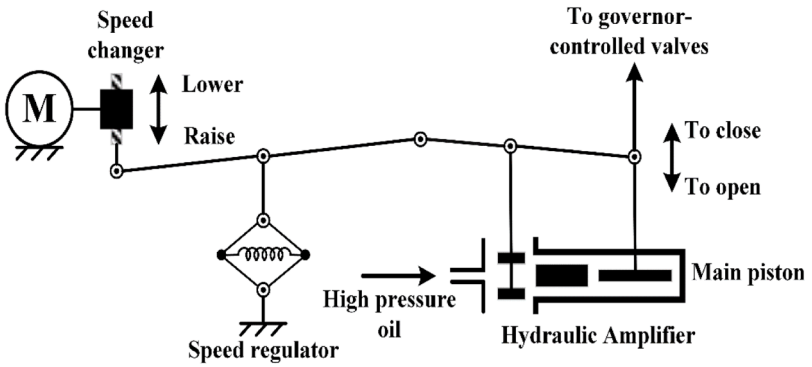

Fig. 1. The outlook of a standard steam turbine.

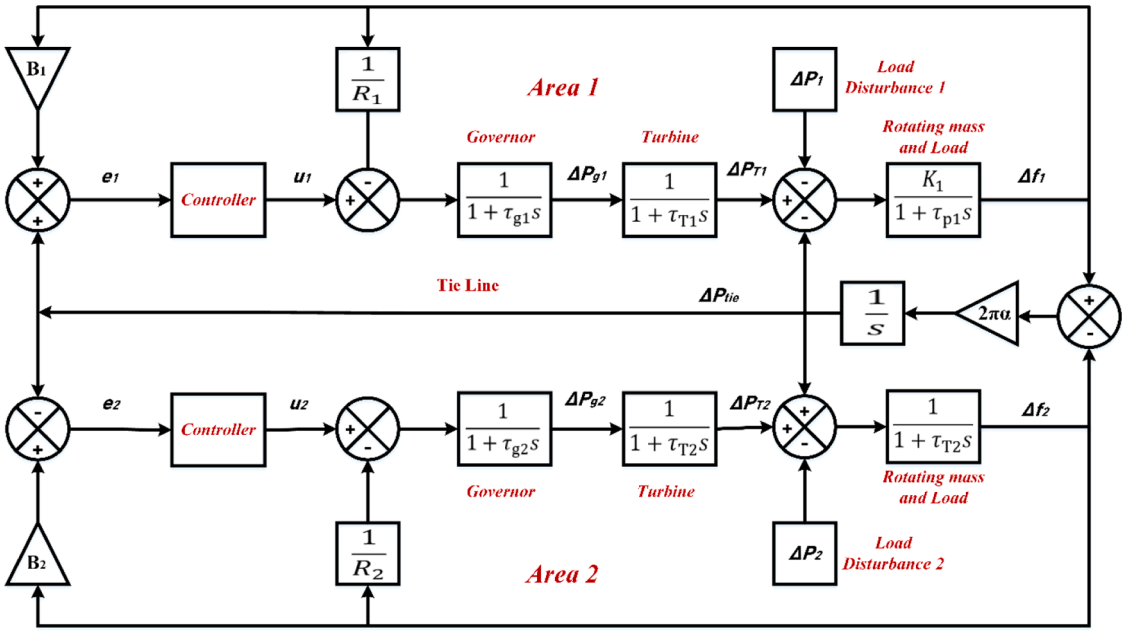

Fig. 2. Two-area grid-connected power system based on transfer function model.

hybrid algorithms that have a higher level of processing time have been gained popularity and are being used widely in industrial applications that require the faster processing time with designing a simpler prototype optimisation control tool [16].

In this paper, a hybrid aquila optimizer-sine-cosine algorithm (HSCAO) that has a faster processing time is employed to address the parameters of a PID-AGC for a two-area power system accurately. To validate the performance and address the parameters of this hybrid algorithm, CEC-2019, and classical benchmark issues with various dimensions are applied. Then, a statistical analysis technique is conducted using Wilcoxon's test and Friedman's test to demonstrate the supervise performance of the HSCAO optimisation regarding to other relative optimising algorithms. Finally, an integral time absolute error (ITAE) performance index is used to calculate the time response of the frequency. Compared to the classical approaches for the FLC-AGC and PID-AGC systems, the robust PID-AGC system's results demonstrate that it quickly restores the frequency level and controls the power delivery of the multi-area power system network under a variety of condition tests because of its quick response and low sensitivity. The rest of paper structure is sorted as follows: The modelling of a two- area power system is explained in Section 2. While, the design of the PID approach based on AGC system is characterized in Sections 3. Next, Section 4 introduces the HSCAO algorithm, whilst Section 5 discusses the proposed PID-AGC method based on the HSCAO algorithm. The major results of the application test are provided in section 6. Finally, Section 7 reports the outcome of this research.

2. Two-area power system modelling

Turbines, generators, and load-demand are the primary components of a grid-power system network. The main function of this system is to use the mechanical energy of the turbine to generate electrical energy in relation to the consumer's load. Usually, steam turbine is employed for these types of the system owing to their higher performance. A governor and reheater are the main outlook part of the steam-turbine, as explained in Fig. 1.

It is work on matching the output energy of the generator with the consumer's load. Consequently, the accelerating turbine changes regulating to the load-consumers by changing the size value of an input steam. As a results, the frequency response will offset from the standard value. Recently, several proposed controls are designed to adjust the speed error of turbine that called the AGC. The speed of the synchronous generator can be calculated mathematically based on Eq. (1):

$$\boldsymbol{\Omega}(\boldsymbol{s}) = \frac{1}{2\boldsymbol{Hs}}(\boldsymbol{\Delta P_m} - \boldsymbol{\Delta P_e}) \tag{1}$$

On the other hand, Eq. (2) is used to calculate the consumer's load.

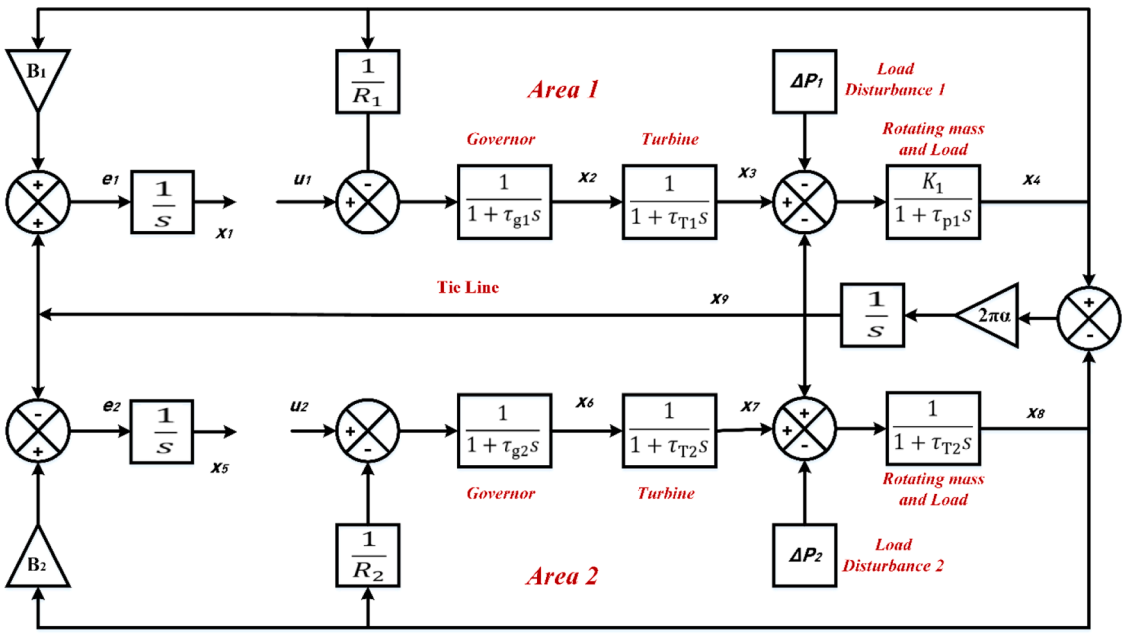

Fig. 3. A power system network of two-are refer to state space approach.

$$\Delta P_e = \Delta P_L + D\Delta\omega \tag{2}$$

To determine the steam turbine, Eq. (3) is utilised:

$$\frac{\Delta P_m(s)}{\Delta P_v(s)} = \frac{1}{1+\tau_T(s)} \tag{3}$$

Finally, Eq. (4) is used to compute the required steam.

$$\Delta P_g = \Delta P_{ref.} - \frac{\Delta\Omega(s)}{R} \tag{4}$$

Eq. (5) indicates how the generator's output power varies with the steam turbine's size:

$$\Delta P_v(s) = \frac{1}{1+\tau_g}\Delta P_g(s) \tag{5}$$

Fig. 2. is represented the block-diagram of two-area power system network based on the transfer function. Then, the state-space equations of system are dravite to get simulation plant.

Typically, each power grid region has a governor, turbine, and load-demand block with a connecting line to its decentral AGC system. For the two-area of a power system network, 9 state equations are constructed for this transfer function. Control input Equations are (6) and (7):

$$\dot{u}_1 = G_1(e_1) = G_1(B_1 x_4 + x_9) \tag{6}$$

$$\dot{u}_2 = G_2(e_2) = G_2(B_2 x_8 - x_9) \tag{7}$$

As seen in Fig. 3, a state-space model for a two-area connected power network has been built, with all 9 states feedback.

Now, the simulation signals of input variable disturbances are represented by ΔP_1 and ΔP_1

Next, Eq. (8-11) show first area state variables:

$$x_1 = \int e_1 \, dt \tag{8}$$

$$x_2 = \Delta P_{g1} \tag{9}$$

$$x_3 = \Delta P_{T1} \tag{10}$$

$$x_4 = \Delta f_1 \tag{11}$$

While the state variables for 2nd area are explained in Eq. (12-15):

$$x_5 = \int e_2 \, dt \tag{12}$$

$$x_6 = \Delta P_{g2} \tag{13}$$

$$x_7 = \Delta P_{T2} \tag{14}$$

$$x_8 = \Delta f_2 \tag{15}$$

Finally, Eq. (16) shows the connected Tie line power of two-area:

$$x_9 = \Delta P_{tie} \tag{16}$$

Then, the rotating mass and load-demand of power grid are represented in Eq. (17-20):

$$x_4 + \tau_{p1}\dot{x}_4 = K_1(x_3 - x_9 - D_1) \tag{17}$$

$$\dot{x}_4 = \frac{K_1}{\tau_{p1}}x_3 - \frac{K_1}{\tau_{p1}}x_4 - \frac{K_1}{\tau_{p1}}x_9 - \frac{K_1}{\tau_{p1}}D_1 \tag{18}$$

$$x_8 + \tau_{p2}\dot{x}_8 = K_2(x_7 - x_9 - D_9) \tag{19}$$

$$\dot{x}_8 = \frac{K_2}{\tau_{p2}}x_7 - \frac{K_2}{\tau_{p2}}x_8 + \frac{K_2}{\tau_{p2}}x_9 - \frac{K_2}{\tau_{p2}}D_1 \tag{20}$$

For steam turbine blocks state space equations are utilised as follows form (21-24):

$$x_3 + \tau_{T1}\dot{x}_3 = x_2 \tag{21}$$

$$\dot{x}_3 = \frac{1}{\tau_{T1}}x_2 - \frac{1}{\tau_{T1}}x_3 \tag{22}$$

$$x_7 + \tau_{T2}\dot{x}_7 = x_6 \tag{23}$$

$$\dot{x}_7 = \frac{1}{\tau_{T2}}x_6 - \frac{1}{\tau_{T2}}x_7 \tag{24}$$

While, Eqs. (26-28) show block governor based on state space approach:

$$x_2 + \tau_{g1}\dot{x}_2 = -\frac{1}{R_1}x_4 + u_1 \tag{25}$$

$$\dot{x}_2 = -\frac{1}{\tau_{g1}}x_2 - \frac{1}{\tau_{g1}R_1}x_4 + \frac{1}{\tau_{g1}}u_1 \tag{26}$$

$$x_6 + \tau_{g2}\dot{x}_6 = -\frac{1}{R_2}x_8 + u_2 \tag{27}$$

$$\dot{x}_6 = -\frac{1}{\tau_{g1}}x_6 - \frac{1}{\tau_{g2}R_2}x_8 + \frac{1}{\tau_{g2}}u_2 \tag{28}$$

Finally, Eq. (29) presents the power system network of the tie line block;

$$\dot{x}_9 = 2\pi\alpha x_8 - 2\pi\alpha x_8 \tag{29}$$

Now, the state equations indicated before may be represented as a single-vector matrix, as shown in Eq. (30).

$$\dot{x} = Ax + Bu + \alpha D \tag{30}$$

where A, also known as the state-matrix, is a demission square matrix. while, the control and disturbance signals are represented by B and α, respectively, which are also the demission matrices. The vector of input state-space is represented by 'x', of 9×1 matrix. The signal of AGC 'u' disturbance 'd' are represented by 2×1 vectors. The total-vectors 'x', 'u', and 'd' can be composited as shown in Eqs. (32-33) at this time.

$$x = [\, x_1 \quad x_2 \quad x_3 \quad x_4 \quad x_5 \quad x_6 \quad x_7 \quad x_8 \quad x_9 \,]^T \tag{31}$$

$$u = \begin{bmatrix} u_1 \\ u_2 \end{bmatrix} D = \begin{bmatrix} D_1 \\ D_2 \end{bmatrix} \tag{32}$$

Now, the 9 state-space equations are finally shown as the following matrices (33–35):

$$A = \begin{bmatrix} 0 & 0 & 0 & B_1 & 0 & 0 & 0 & 0 & 1 \\ 0 & \frac{-1}{\tau_{g1}} & 0 & \frac{-1}{\tau_{g1}R_1} & 0 & 0 & 0 & 0 & 0 \\ 0 & \frac{K_1}{\tau_{p1}} & \frac{-K_1}{\tau_{p1}} & 0 & 0 & 0 & 0 & 0 & 0 \\ 0 & 0 & \frac{1}{\tau_{T1}} & \frac{-1}{\tau_{T1}} & 0 & 0 & 0 & 0 & \frac{1}{\tau_{T1}} \\ 0 & 0 & 0 & 0 & 0 & 0 & 0 & B_2 & 1 \\ 0 & 0 & 0 & 0 & 0 & \frac{-1}{\tau_{g2}} & 0 & \frac{-1}{\tau_{g2}R_2} & 0 \\ 0 & 0 & 0 & 0 & 0 & \frac{1}{\tau_{t2}} & \frac{-1}{\tau_{t2}} & 0 & 0 \\ 0 & 0 & 0 & 0 & 0 & 0 & \frac{K_1}{\tau_{p2}} & \frac{-K_1}{\tau_{p2}} & 0 \\ 0 & 0 & 0 & 2\pi\sigma & 0 & 0 & 0 & 2\pi\sigma & 0 \end{bmatrix} \tag{33}$$

$$B = \begin{bmatrix} 0 & 0 \\ \frac{1}{\tau_{g1}} & 0 \\ 0 & 0 \\ 0 & 0 \\ 0 & 0 \\ 0 & \frac{1}{\tau_{g2}} \\ 0 & 0 \\ 0 & 0 \\ 0 & 0 \end{bmatrix} \tag{34}$$

$$\alpha = \begin{bmatrix} 0 & 0 \\ 0 & 0 \\ 0 & 0 \\ \frac{-K_1}{\tau_{p1}} & 0 \\ 0 & 0 \\ 0 & 0 \\ 0 & 0 \\ 0 & \frac{-K_1}{\tau_{p2}} \\ 0 & 0 \end{bmatrix} \tag{35}$$

This state space equations will be used in the proposed algorithm code to find the accurate parameters of the PID-AGC control system.

3. A PID controller based on AGC

The PID controller is considered the most common type in manufacturing implementations owing to its simplicity and fastness. In addition, it does not require accurate model of the plant and can be understood by most engineers without being a controlling expert. However, it is not efficient for a highly dynamic variation time of processing plant such as AGC. The conventional of PID controller based on AGC can be expressed mathematically in Eq. (36):

$$u(t) = K_p ACE + K_i \int ACE dt + K_d \frac{dACE}{d(t)} \tag{36}$$

In contrast, ACE stands for processing plant error, which can be expressed mathematically as Eq. (37):

$$e(t) = \Delta P_{tie} + \beta \Delta f \tag{37}$$

Addressing the values of Kp, Ki and Kd are the major challenge to employ the robust PID controller in industrial plant. Consequently, the regulating of PID controller is the essential step to implement the efficient PID controller. Generally, there are two methods to tune the elements of PID controller; try and error and Ziegler-Nichols. However, those methods are not suitable for the processing Plant that has a highly dynamic fluctuation such as the power system network. Hence, several researchers have investigated the optimisation techniques to adjust the parameters of PID controller. In this work, the HSCAO algorithm is utilised to address the parameters of PID controller adequately. Then, the robust PID controller is assessed under ITAE performance index method to determine the transient response time of the system under external disturbances.

4. Optimisation algorithms

4.1. Standard SCA algorithm

The SCA is described in ref. [17] to employ the characteristics of the trigonometric function's sine and cosine that have been used to address the best candidate solutions. The fluctuating factors of a since cosine mathematical model are used to evaluate the best candidate solutions. Based on the likelihood that the global optimum will increase, it looks for optimization problems with an adequate number of random solutions and optimization steps. Hence, the following equations are the definitions of the search equations utilised in SCA to determine the position of candidate solutions:

$$Y_i^{g+1} = Y_i^t + r_1 \sin(r_2) \times \left| r_3 P_i^t - Y_i^t \right| \tag{38}$$

$$Y_i^{t+1} = Y_i^t + r_1 \cos(r_2) \times \left| r_3 P_i^t - Y_i^t \right| \tag{39}$$

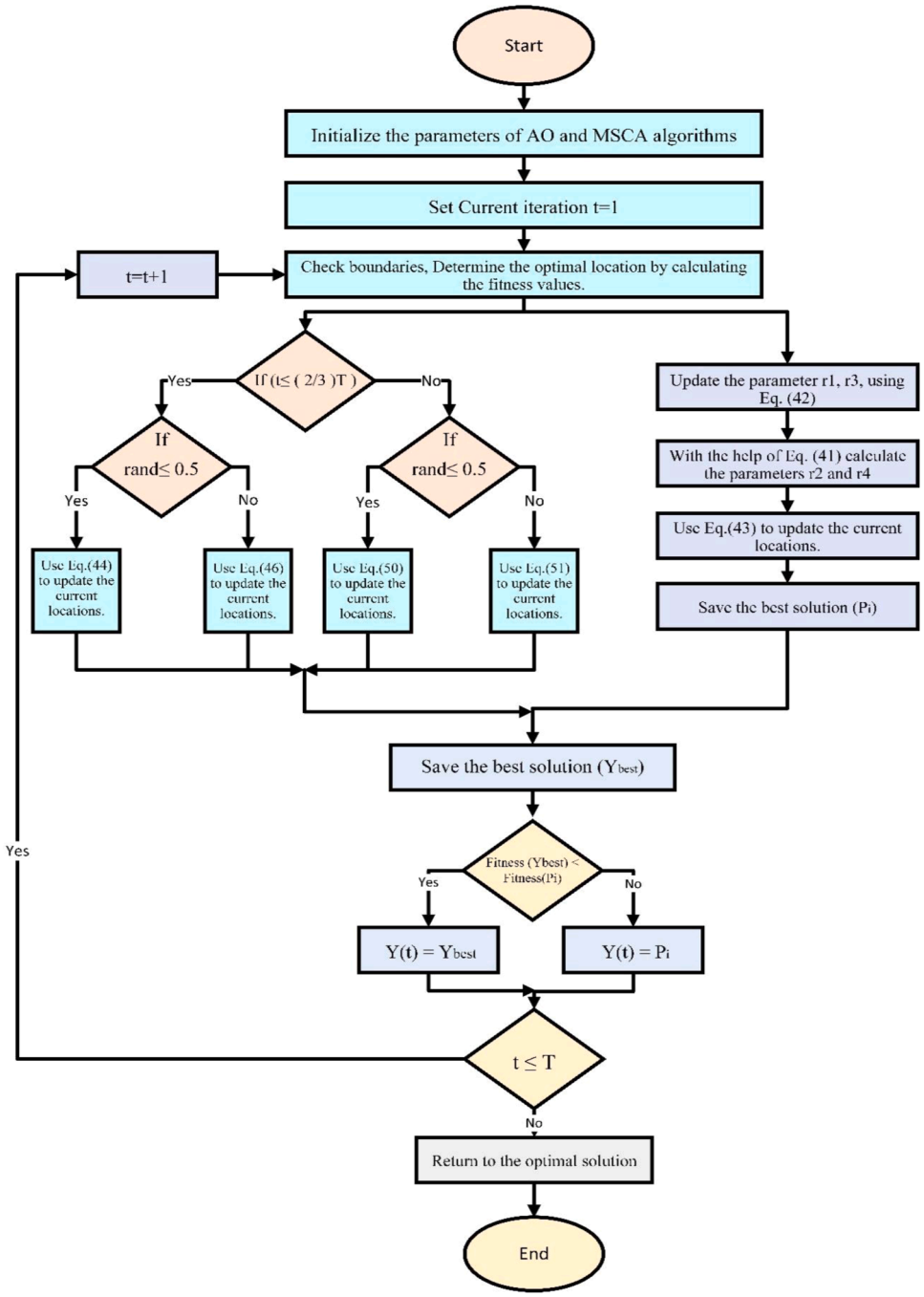

Fig. 4. The flowchart of HSCAO algorithm.

Those Equations are used in the SCA methodology as follows:

$$Y_i^{t+1} = \begin{cases} Y_i^t + r_1 sin\,(r_2) \times \left| r_3 P_i^t - V_i^t \right|, r_4 < 0.5 \\ Y_i^t + r_1 cos\,(r_2) \times \left| r_3 P_i^t - V_i^t \right|, r_4 \geq 0.5 \end{cases} \tag{40}$$

The parameter r_1 is the potential area where the solution and the target can be positioned, potentially within a specific region. This parameter allows for the examination and utilisation of a search area while maintaining an optimal balance between them. The process divides the maximum iteration count in half, allocating one half to diversification and the other half to enhancing exploration within a feasible search area [18]. The parameter r_2 determines the orientation of the moment for a particular solution. The parameter r_3 quantifies the significance of the weight assigned to P_i^t. By manipulating the parameter r_4, Eq. (41) facilitates the transition from sine to cosine functions. The mathematical updates for the parameters r_1, r_2, r_2, and r_4 are as following:

$$\begin{cases} r_1 = a - a \times \dfrac{t}{T} \\ r_2 = (2 \times \pi) \times rand \\ r_3 = 2 \times rand \\ r_4 = rand \end{cases} \tag{41}$$

Table 1
Unimodal and multimodal test functions.

Problems	Objective Function	Range	f_{min}	D
F1	$f(x) = \sum_{i=1}^{n} x_i^2$	[-100,100]	0	10,30
F2	$f(x) = \sum_{i=0}^{n} \lvert x_i \rvert + \prod_{i=0}^{n} \lvert x_i \rvert$	[-10,10]	0	10,30
F3	$f(x) = \sum_{i=1}^{d} \left(\sum_{j=1}^{i} x_j \right)^2$	[-100,100]	0	10,30
F4	$f(x) = \max_i \{ \lvert x_i \rvert, 1 \le i \le n \}$	[-100,100]	0	10,30
F5	$f(x) = \sum_{i=1}^{n=1} \left[100 \left(x_i^2 - x_{i+1} \right)^2 + (1 - x_i)^2 \right]$	[-30,30]	0	10,30
F6	$f(x) = \sum_{i=1}^{n} (\lvert x_i + 0.5 \rvert)^2$	[-100,100]	0	10,30
F7	$f(x) = \sum_{i=0}^{n} i x_i^4 + \text{random}[0,1)$	[-128,128]	0	10,30
F8	$f(x) = \sum_{i=1}^{n} \left(- x_i \sin \left(\sqrt{\lvert x_i \rvert} \right) \right)$	[-500,500]		10,30
F9	$f(x) = \sum_{i=1}^{n} \left[x_i^2 - 10\cos(2\pi x_i) + 10 \right]$	[-5.12,5.12]	0	10,30
F10	$f(x) = -20\exp\left(-0.2\sqrt{\frac{1}{n}\sum_{i=1}^{n} x_i^2} \right) - \exp\left(\frac{1}{n}\sum_{i=1}^{n} \cos(2\pi x_i) \right) + 20 + e$	[-32,32]	0	10,30
F11	$f(x) = 1 + \frac{1}{4000}\sum_{i=1}^{n} x_i^2 - \prod_{i=1}^{n} \cos\left(\frac{x_i}{\sqrt{i}} \right)$	[-600,600]	0	10,30
F12	$f(x) = \frac{\pi}{n}\{10\sin(\pi y_1)\} + \sum_{i-1}^{n-1} (y_i - 1)^2 \left[1 + 10\sin^2(\pi y_{i+1}) \right] + \sum_{i=1}^{n} u(x_i, 10, 100, 4)$, where $y_i = 1 + \frac{x_i + 1}{4}$, $u(x_i, a, k,$ $m) \{ K(x_i - a)^m \ if \ x_i > a \ ; \ 0 \ -a \le x_i \ge a \ ; \ K(-x_i - a)^m \ -a \le x_i$	[-50,50]	0	10,30
F13	$f(x) = 0.1 \Big(\sin^2(3\pi x_1) + \sum_{i=1}^{n} (x_i - 1)^2 [1 + \sin^2(3\pi x_i + 1)] + (x_n - 1)^2 1 + \sin^2(2\pi x_n)) + \sum_{i=1}^{n} u(x_i, 5, 100, 4)$	[-50,50]	0	10,30

Table 2
Comparative algorithm parameters.

Algorithm	Parameter	Value
SCA [16]	A	2
WOA [23]	A	Decreased from 2 to 0
	B	2
SMA [24]	v_b and v_c	Decreased from 2 to 0
EO [25]	r	0.5
	a	4
	GP	0.5
AO [20]	α	0.1
	δ	0.1
AOA [26]	α	5
	μ	0.5
MHA [27]	bp	0.05
	R	[0,1]
	P	exp
	l	Decreased from -2 to -1
	t	Decreased from 2 to 0
	CF	*adaptive*
	Λ	*sa*
NMRA [28]	bp	0.5
	Λ	[0,1]
MFO [29]	b	1
	t	[-1,1]
GWO [30]	A	Decreased from 2 to 0
MPA [31]	R	[0,1]
	P	0.5

4.2. Modified Sine Cosine Algorithm (MSCA)

For meta-heuristic algorithms to grow increasingly proficient at producing results, they must maintain a balanced strategy between exploration and exploitation throughout the search process. However, other studies have shown that the SCA commonly fails to maintain this balance [19]. Particularly, when handling multimodal challenges of the classic SCA strategy has a tendency to overemphasise diversity at the expense of proper exploitation [18]. Only the best answer is kept for the next iteration in the typical SCA method, where all prior solutions are totally replaced with new ones with each iteration. Ineffective algorithmic exploration results from this method's failure to take into account the potential contributions of individual solutions in defining effective search pathways. To address this issue, two modifications are suggested for the conventional SCA algorithm, these modifications involve the updated parameters, namely, r_1 and r_3 in Eq. (41), as well as an enhanced search equation to improve the overall performance of the algorithm by reaching a more accurate balance between exploration and exploitation. A new general set of parameters, r_1 and r_3, are produced by modifying Eq. (42) as following:

$$\begin{cases} \boldsymbol{r}_1 = 1 - \left(\dfrac{\boldsymbol{t}}{\boldsymbol{T}} \right)^{\alpha \times \frac{\boldsymbol{t}}{\boldsymbol{T}}} \\ \boldsymbol{r}_3 = \boldsymbol{r}_1 \times rand \end{cases} \tag{42}$$

In the second modification, the current solution Y_i^t in the first section is replaced with the most optimal solution P_i^t. By implementing this modification, the algorithm gains the ability to efficiently explore areas that show potential in close proximity to the individual optimal solutions. This adjustment is beneficial in cases where the optimal solution is limited to a specific area and does not offer sufficient guidance for the search process. Consequently, the Modified Eq. (40) can be formulated in the following manner:

$$\boldsymbol{Y}_i^{g+1} = \begin{cases} \boldsymbol{P}_i^t + \boldsymbol{r}_1 sin\ (\boldsymbol{r}_2) \times \left| \boldsymbol{r}_3 \boldsymbol{P}_i^t - \boldsymbol{Y}_i^t \right|, r_4 < 0.5 \\ \boldsymbol{P}_i^t + \boldsymbol{r}_1 cos\ (\boldsymbol{r}_2) \times \left| \boldsymbol{r}_3 \boldsymbol{P}_i^t - \boldsymbol{Y}_i^t \right|, r_4 \ge 0.5 \end{cases} \tag{43}$$

4.3. Aquila Optimizer (AO)

In 2021, Abualigah et al.[20] introduced Aquila Optimizer such as advanced algorithm based on swarm intelligence. This algorithm draws inspiration from the versatile hunting tactics of the Aquila, which can be skilfully adapted its predatory methods based on the different types of prey. It hints its target with four potent behaviours: walking and grabbing prey, contour fighting with a brief glide assault, low fighting with a slow fall attack, and high soaring with a vertical stoop. Therefore, four mathematical model have been utilised to explain the procedure of the AO algorithm

- Expanded Exploration (Y_1)

Table 3
Results of the test functions (F1-F13) based on classical benchmark problems.

Fun No.	Measure	Comparative optimisation algorithms						
		HSCAO	AO	MSCA	SCA	SMA	EO	WOA
$f_1(x)$	Best	**0**	5.9145E-301	2.3356E-248	1.2270E-34	**0**	1.6105E-144	4.3834E-173
	Worst	0	7.9371E-200	5.5187E-236	6.6359E-26	0	2.7010E-137	2.6941E-152
	Average	0	3.9686E-201	2.7595E-237	4.8680E-27	0	1.3822E-138	1.3471E-153
	STD	0	0	0	1.5188E-26	0	6.0328E-138	6.0242E-153
$f_2(x)$	Best	**0**	1.1539E-152	6.6255E-137	6.6060E-23	**0**	5.8528E-117	1.5350E-79
	Worst	0	1.5199E-99	4.3851E-132	2.2576E-18	1.1649E-182	3.0855E-106	5.3533E-76
	Average	0	1.0906E-100	2.4369E-133	3.4186E-19	5.8243E-184	1.5747E-107	7.1710E-77
	STD	0	3.6326E-100	9.7715E-133	6.2318E-19	0	6.8925E-107	1.4403E-76
$f_3(x)$	Best	**0**	9.6912E-300	3.8680E-157	4.0471E-15	**0**	1.1853E-78	1.1640E-03
	Worst	0	1.4199E-190	5.2990E-135	8.3518E-07	0	2.9019E-68	2.7236E+02
	Average	0	7.0995E-192	2.6495E-136	4.8068E-08	0	3.4564E-69	2.4649E+01
	STD	0	0	1.1849E-135	1.8710E-07	0	7.9752E-69	6.1582E+01
$f_4(x)$	Best	**2.6714e-273**	5.0737e-80	6.9726E-13	5.0080E+01	3.1872E-271	2.2224E-08	1.1909E+00
	Worst	1.2796e-187	3.2349e-52	9.2911 E+01	7.7751E+01	4.1925E-146	3.2840E-06	9.3667E+01
	Average	6.5053e-189	1.6174e-53	4.6455 E+00	6.6715E+01	2.0963E-147	5.0470E-07	6.7158E+01
	STD	0	7.2335e-53	2.0775E+01	6.9172E+00	9.3749E-147	7.0982E-07	2.5579E+01
$f_5(x)$	Best	**4.5723E-07**	3.9738E-06	5.9106E+00	6.5350E+00	9.5098E-06	4.0683E+00	5.6791E+00
	Worst	1.4431E-03	5.5662E-03	8.0561E+00	5.7169E+02	2.1006E-02	4.7033E+00	8.5339E+00
	Average	6.4192E-03	5.9230E-04	6.6091E+00	3.5465E+01	4.8222E-03	4.3129E+00	6.2874E+00
	STD	2.0380E-03	1.2250E-03	5.4860E-01	1.2621E+02	6.3066E-03	1.8169E-01	6.2250E-01
$f_6(x)$	Best	2.0736E-09	2.5533E-07	9.9369E-03	1.6607E-01	3.3763E-06	**0**	1.4837E-05
	Worst	3.4706E-05	1.2922E-04	7.5461E-01	7.9726E-01	3.8534E-05	4.9304E-32	1.3158E-04
	Average	2.8458E-06	1.2807E-05	1.8074E-01	4.0811E-01	1.2197E-05	4.0059E-33	5.9341E-05
	STD	7.8284E-06	2.8784E-05	2.1228E-01	1.6358E-01	9.5215E-06	1.1315E-32	3.4797E-05
$f_7(x)$	Best	**8.9027E-06**	6.5528E-06	4.3670E-05	5.6417E-05	2.9416E-06	2.8094E-05	7.4159E-05
	Worst	2.0313E-04	1.3826E-04	7.8264E-04	9.2785E-03	3.6715E-04	1.0876E-03	3.9658E-03
	Average	6.2305E-05	5.0675E-05	2.2082E-04	1.7889E-03	7.0059E-05	2.6544E-04	9.3760E-04
	STD	5.4427E-05	3.4201E-05	1.8254E-04	2.0821E-03	8.3717E-05	2.6916E-04	1.0556E-03
$f_8(x)$	Best	-4.1885E+03	-4.1895E+03	-2.6979E+03	-2.6929E+03	**-4.1898E+03**	-3.8329E+03	-4.1897E+03
	Worst	-2.1936E+03	-2.3241E+03	-1.4873E+03	-1.9536E+03	-4.1898E+03	-2.6410E+03	-2.8098E+03
	Average	-2.8955E+03	-3.8775E+03	-2.1363E+03	-2.2631E+03	-4.1898E+03	-3.2654E+03	-3.6872E+03
	STD	4.8923E+02	6.4494E+02	2.9835 E+02	2.2357 E+02	3.2277E-04	3.1937 E+02	5.5428E+02
$f_9(x)$	Best	**0**	**0**	**0**	**0**	**0**	**0**	**0**
	Worst	0	0	1.7536E+01	1.9643E+01	0	2.9848E+00	0
	Average	0	0	1.5207 E+00	9.8216E+01	0	1.4924E+01	0
	STD	0	0	4.7414 E+00	4.3923 E+00	0	6.6743 E+00	0
$f_{10}(x)$	Best	**8.8817E-16**	**8.8817E-16**	4.4408E-15	**8.8817E-16**	8.8817E-16	4.4408E-15	**8.8817E-16**
	Worst	8.8817E-16	8.8817E-16	4.4408E-15	1.6431E-13	8.8817E-16	4.4408E-15	7.9936E-15
	Average	8.8817E-16	8.8817E-16	4.4408E-15	2.6467E-14	8.8817E-16	4.4408E-15	3.5527E-15
	STD	0	0	0	4.2983E-14	0	0	2.2689E-15
$f_{11}(x)$	Best	**0**	**0**	**0**	**0**	**0**	**0**	**0**
	Worst	0	0	2.7502E-01	6.4433E-01	0	7.3960E-02	5.1852E-01
	Average	0	0	4.3885E-02	9.928E-02	0	3.6980E-04	1.0211 E-01
	STD	0	0	6.9274E-02	2.1211E-02	0	1.6538E-03	1.6596 E-01
$f_{12}(x)$	Best	**1.5453E-10**	1.5792E-08	3.0484E-01	3.101E+00	2.9682E-05	2.1707E-05	1.3380E-02
	Worst	9.7415E-06	1.4132E-05	6.2344E-01	3.6874E+07	2.7446E-02	4.0713E-03	1.6532E-01
	Average	1.5175E-06	1.3506E-06	3.9866E-01	6.1011E+06	7.3348E-03	4.7975E-04	4.1710E-02
	STD	2.2800E-06	3.1726E-06	8.4381E-02	9.8604E+06	8.0396E-03	1.1759E-03	4.1869E-02
$f_{13}(x)$	Best	**1.0048e-08**	1.9525E-07	3.2990E+00	5.4730E+05	2.3113E-04	1.0236E-01	3.8002E-01
	Worst	1.4107E-04	3.7256E-04	4.2090E+00	6.5514E+07	1.4377E-01	1.1164E+00	2.1803E+00
	Average	1.0344e-05	4.0321E-05	3.7807E+00	2.1261E+07	2.5438E-02	5.6873E-01	1.2201E+00
	STD	3.0998e-05	9.0754E-05	2.0368E-01	1.6957E+07	3.3696E-02	3.0347E-01	5.6001E-01
(W|L|T)		(5|2|6)	(0|9|4)	(0|11|2)	(0|10|3)	(1|7|5)	(1|10|2)	(0|10|3)
Mean		2.1923	2.8461	5.0384	6.0769	2.5769	4.3465	4.9230
Ranking		1	3	6	7	2	4	5

In the first step, the initial approach (Y_1) involved the Aquila identifying the location of its prey and subsequently choosing an ideal hunting area by ascending to an elevated position with a prominent hump. The behaviour of Aquila uses as the mountain view to explore the search area that is mathematically represented as the following equation:

$$\boldsymbol{Y}_1(\boldsymbol{t}+1) = \boldsymbol{Y}_{\boldsymbol{best}}(\boldsymbol{t}) \times \left(1 - \frac{\boldsymbol{t}}{\boldsymbol{T}}\right) + \left(\boldsymbol{Y}_{\boldsymbol{M}}(\boldsymbol{t}) - \boldsymbol{Y}_{\boldsymbol{best}}(\boldsymbol{t}) \times \mathbf{rand}\right) \tag{44}$$

$$\boldsymbol{Y}_{\boldsymbol{M}}(\boldsymbol{t}) = \frac{1}{\boldsymbol{N}} \sum_{i=1}^{\boldsymbol{N}} \boldsymbol{Y}_i(\boldsymbol{i}), \forall \boldsymbol{j} = 1, 2, \ldots, \boldsymbol{Dim} \tag{45}$$

• Narrowed Exploration (Y_2)

In the second step, the most popular method of Aquila hunting is addressed. It includes a brief glide to attack the prey subsequent to descending and encircling it within the specified area. Eq. (9) can be represented this behaviour mathematically.

$$\boldsymbol{Y}_2(\boldsymbol{t}+1) = \boldsymbol{Y}_{\boldsymbol{best}}(\boldsymbol{t}) \times \mathbf{LF}(\mathbf{D}) + \boldsymbol{Y}_{\boldsymbol{R}}(\boldsymbol{t}) + (\boldsymbol{z} - \boldsymbol{h}) \times \mathbf{rand}) \tag{46}$$

The solution for the subsequent iteration, denoted as $Y_2(t+1)$, is obtained using the second search method, also known as contour flight with a short glide attack. This solution exists within a dimensional space denoted by D. A key component in this computation is the Levy flight distribution function, represented as LF(D), which can be calculated using Eq. (47). The method also employs a random solution $Y_R(t)$, selected within the range of [N] during the ith iteration.

Table 4
Results using classical test functions (F1-F13) (D= 30) compared with the relative optimal algorithms.

Fun No.	Measure	Comparative optimisation algorithms						
		HSCAO	MHA	NMRA	MPA	WOA	GWO	MFO
$f_1(x)$	Average	0	0	1.12E-86	5.05E-23	1.11E-83	3.14E-33	1.17E+03
	STD	0	0	7.88E-86	4.93E-23	7.37E-83	5.32E-32	3.25E+03
$f_2(x)$	Average	7.63E-205	1.63E-180	3.46E-45	3.08E-13	1.88E-54	7.11E-20	3.11E+01
	STD	0	0	1.52E-44	2.98E-13	5.69E-54	6.53E-20	2.00E+01
$f_3(x)$	Average	0	1.16E-318	2.54E-85	6.71E-05	2.97E+04	3.85E-08	1.89E+04
	STD	0	0	1.32E-84	1.37E-04	9.33E+03	6.91E-08	1.23E+04
$f_4(x)$	Average	3.85E-201	1.00E-185	3.50E-45	3.15E-09	3.72E+01	2.18E-08	6.03E+01
	STD	0	0	1.52E-44	1.75E-09	2.87E+01	1.74E-08	9.31E+00
$f_5(x)$	Average	2.01E-03	2.84E+01	2.89E+01	2.45E+01	2.74E+01	2.67E+01	1.32E+04
	STD	3.55E-03	3.23E-01	2.54E-02	4.37E-01	4.79E-01	6.86E-01	3.11E+04
$f_6(x)$	Average	9.33E-06	3.86E-01	6.56E+00	1.43E-08	8.45E-02	4.70E-01	5.92E+02
	STD	1.36E-05	1.28E-01	5.90E-01	6.25E-09	1.20E-01	2.77E-01	2.38E+03
$f_7(x)$	Average	1.59E-04	9.65E-05	6.94E-04	1.00E-03	2.30E-03	1.20E-03	3.02E+00
	STD	1.30E-04	1.19E-04	6.10E-04	4.32E-04	2.70E-03	5.08E-04	7.37E+00
$f_9(x)$	Average	0	0	0	0	1.11E-15	1.64E+00	1.52E+02
	STD	0	0	0	0	7.95E-15	3.06E+00	3.04E+01
$f_{10}(x)$	Average	8.88E-16	8.88E-16	8.88E-16	1.44E-12	4.44E-15	4.26E-14	1.16E+01
	STD	0	0	0	8.94E-13	2.24E-15	3.32E-15	8.60E+00
$f_{11}(x)$	Average	0	0	0	0	4.28E-02	8.60E-03	5.70E-03
	STD	0	0	0	0	6.70E-02	3.46E-02	2.85E-02
$f_{12}(x)$	Average	6.40E-07	1.65E-02	1.09E+00	1.39E-09	7.40E-03	2.59E-02	5.32E+00
	STD	1.05E-06	8.20E-03	2.56E-01	6.50E-10	6.30E-03	1.31E-02	6.64E+00
$f_{13}(x)$	Average	1.22E-05	2.69E-01	2.97E+00	6.53E-04	2.25E-01	3.34E-01	8.02E+00
	STD	2.43E-05	8.12E-02	1.38E-01	2.60E-03	1.60E-01	2.02E-01	7.71E+00

$$\mathbf{LF}(\mathbf{D}) = 0.01 \times \frac{\boldsymbol{u} \times \boldsymbol{\sigma}}{|\boldsymbol{v}|^{\frac{1}{\beta}}} \tag{47}$$

$$\boldsymbol{\sigma} = \frac{\boldsymbol{\Gamma}(1+\boldsymbol{\beta}) \times \mathbf{sinc}\left(\frac{\pi\beta}{2}\right)}{\boldsymbol{\Gamma}\left(\frac{1+\beta}{2}\right) \times \boldsymbol{\beta} \times 2^{\frac{\beta-1}{2}}} \tag{48}$$

The values u and υ are generated at random from 0 to 1. Where β is a fixed value that is established at 1.5. The spiral shape in the search is represented by z and h in Eq. (49), these values are computed as follows:

$$\begin{cases} z = k \times \sin(\phi) \\ h = k \times \cos(\phi) \\ k = \boldsymbol{r}_5 + 0.00565 \times \boldsymbol{D}_1 \\ \phi = -0.05 \times \boldsymbol{D}_1 + \dfrac{3 \times \boldsymbol{\pi}}{2} \end{cases} \tag{49}$$

where r_5 is ranging the search cycles from 1 to 20, while, D_1 is an integer numbers between 1 and dimension size.

• Expanded exploitation (Y_3)

In this step, the Aquila addresses the position of its prey, then, it descends vertically for an initial attack, reducing its speed if the prey is spotted which is known as the low-altitude and descent attack. This method involves the Aquila precisely designating the prey area, preparing for landing, and initiating an attack. The Aquila uses the selected area as its method vector for getting close to and attacking the prey. This behaviour, which involves observing the prey's response to the initial attack, is mathematically represented as in Eq. (50).

$$\boldsymbol{Y}_3(\boldsymbol{t}+1) = (\boldsymbol{Y}_{\boldsymbol{best}}(\boldsymbol{t}) - \boldsymbol{Y}_{\boldsymbol{M}}(\boldsymbol{t})) \times \alpha - \mathbf{rand} + ((\boldsymbol{Ub} - \boldsymbol{Lb}) \times \mathbf{rand} + \mathbf{Lb}) \times \delta \tag{50}$$

• Narrowed exploitation (Y_4)

In the pursuit and capture strategy, Aquila in this approach follows the prey, taking into account its potential escape direction, and subsequently launches an assault on the terrestrial target. This behaviour can be presented to mathematical expression as follows.

$$\boldsymbol{Y}_4(\boldsymbol{t}+1) = \boldsymbol{QF} \times \boldsymbol{Y}_{\boldsymbol{best}}(\boldsymbol{t}) - (\boldsymbol{G}_1 \times \mathbf{Y}(\mathbf{t}) \times \mathbf{rand}) - \boldsymbol{G}_2 \times \mathbf{LF}(\mathbf{D}) + \mathbf{rand} \times \boldsymbol{G}_1 \tag{51}$$

$$\boldsymbol{QF}(\boldsymbol{t}) = \boldsymbol{t}^{\frac{G_1}{(1-T)^2}} \tag{52}$$

$$\begin{cases} \boldsymbol{G}_1 = 2 \times rand - 1 \\ \boldsymbol{G}_2 = 2 \times \left(1 - \dfrac{\boldsymbol{t}}{\boldsymbol{T}}\right) \end{cases} \tag{53}$$

The function QF(t) is used to harmonize the search approach. In other side, the parameter of G_1 tracks the prey's movements of Aquila that is taking a random value from the inclusive range [-1, 1]. While, G_2 represents the decline in flight incline as Aquila pursues its prey, with a linear reduction.

4.4. Hybrid AO and MSCA algorithms

The Aquila Optimizer (AO) [20] is a swarm intelligence algorithm that replicates four foraging strategies which is inspired by the predation behavior of Aquila. It has a rapid convergence, high search efficiency, and robust global exploration capability [21]. However, it has been observed that the AO has insufficient local exploitation capability and is prone to falling into local optima, leading to premature convergence [22]. The experimental findings for the Modified Sine Cosine Algorithm (MSCA) indicate weaknesses in population diversification and slow convergence speed during the exploration phase, also faces challenges in handling complex problems with high dimensional features. Despite the modifications, it still struggles with certain optimization problems. To address these shortcomings, a new hybrid algorithm, the Hybrid Aquila Optimizer-based Sine Cosine Algorithm (HSCAO), is proposed. This algorithm combines the strengths of the AO and MSCA, aiming to leverage the advantages of both algorithms while mitigating their inherent disadvantages.

The HSCAO algorithm is designed to offer a better solution for addressing the challenges faced by traditional optimization algorithms in the domains which requires high convergence speed with better performance. The HSCAO algorithm operates by running the AO and

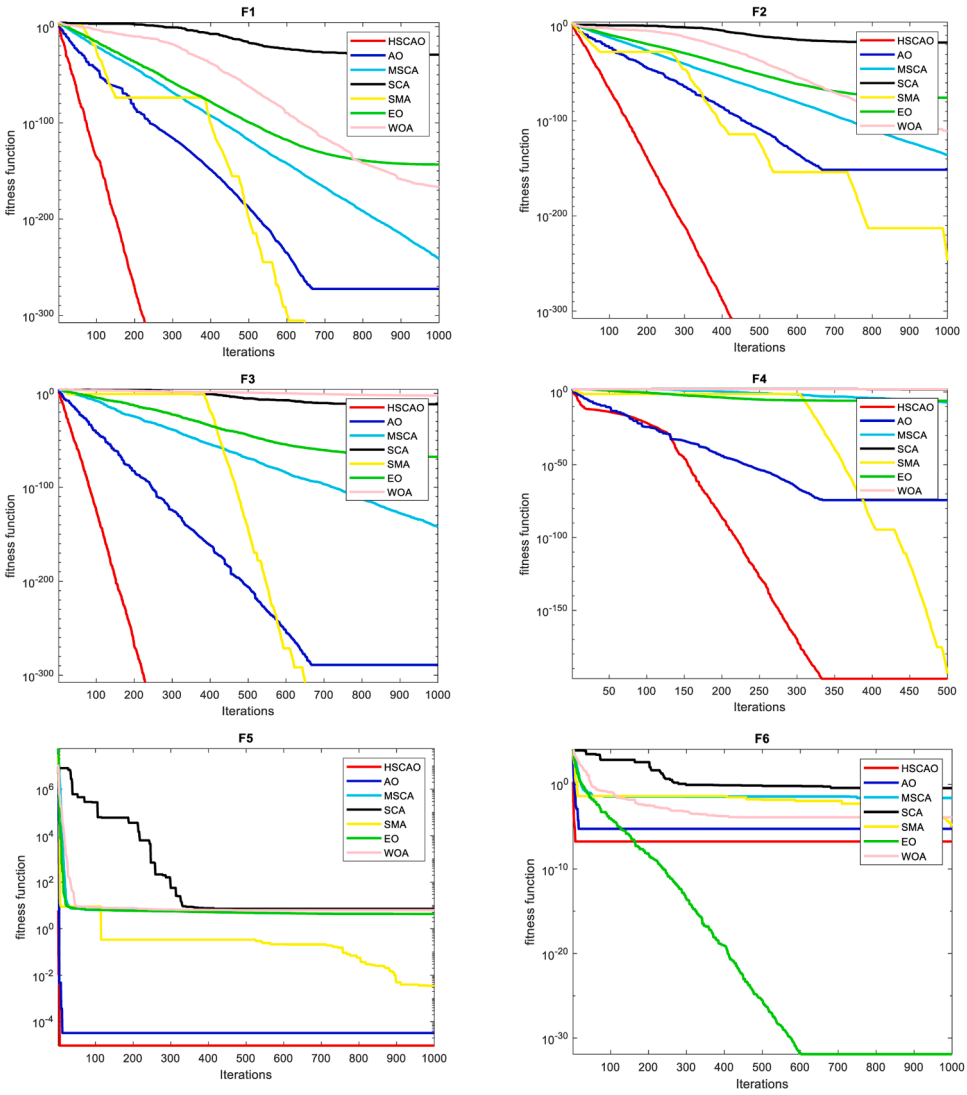

Fig. 5. Convergence patterns of various algorithms in comparison based on classical issues.

MSCA in parallel, with each algorithm operating on its own population of solutions. To avoid the insufficient exploitation phase of the AO method, the fact that the exploration phase is implemented at the first step of the proposed algorithm around 2/3 of the iteration. Hence, the effective intensification phase of MSCA is implemented in place of the AO's restricted exploration phase. Consequently, the objective is to accelerate the process of achieving the optimal solution by enhancing the exploitation stage of the hybrid HSCAO. After each iteration, the algorithm compares the best solution found by each method and updates a global best solution variable accordingly. This approach ensures that the advantages of both algorithms are utilized and the best solution is selected based on the fitness function value. The flowchart of the proposed algorithm is shown its major steps, as presented in Fig. 4. In the first stage, the initial parameters of the HSCAO algorithm are set. Then, the optimal location of boundaries is calculated based on fitness functions. In the AO method, the exploitation phase is insufficient to despite the fact of the exploration phase at 2/3 of the iteration. In order to prioritize the exploitation capability, the effective intensification phase of MSCA is implemented in place of the AO's restricted exploration phase. Consequently, the objective is accelerated the process of the optimal solution by enhancing the exploitation stage of the hybrid HSCAO. This algorithm will be used to enhance the performance of the PID-AGC system based on addressing the optimal parameters of the PID control.

5. Proposed HSCAO algorithm based on AGC

The findings and analysis related to the suggested HSCAO are presented in this section, and its comparisons with respect to other algorithms based on AGC. Four subsections make up this section. Comprehensive details regarding the benchmark functions and comparative algorithms used to assess the suggested algorithm's performance are given in the first subsection. To give the sensitivity analysis of the suggested approach, comprehensive results on traditional benchmark problems are shown in the second subsection, resulting in, the improved parameter fits of the HSCAO algorithm. To demonstrate the impact of the suggested algorithm comparison with the relative optimal algorithms, the third subsection examines CEC 2019 benchmark challenges which is considered more challenge. In the fourth subsection, the optimization issue instances in the PID-AGC system's tuning parameters are finally presented based on a fitness function.

5.1. Parameter settings and the test suite

This section provides extensive details about the classical benchmark suite used for the analysis of proposed algorithm. The benchmark suite

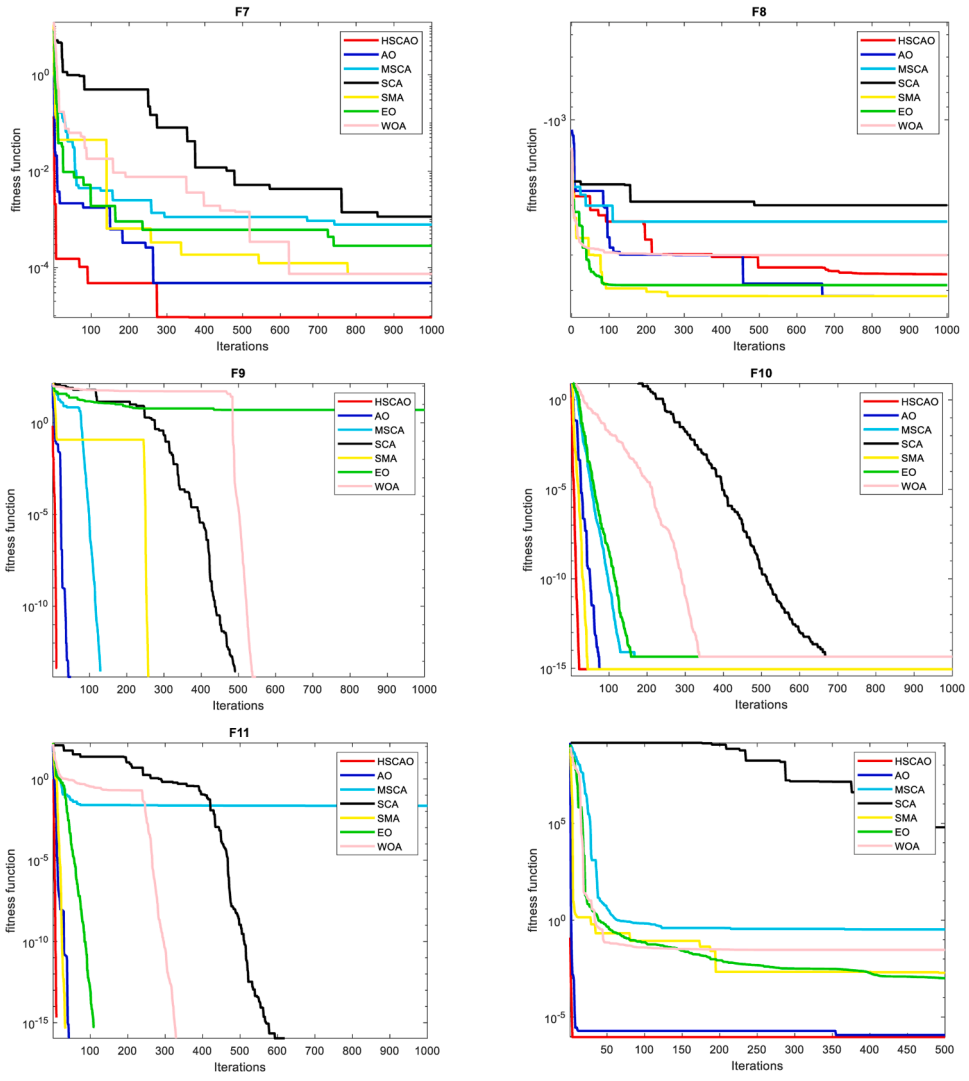

Fig. 5. (*continued*).

consists of thirteen classical problems that its problems are unimodal and multimodal problems, with variable dimension sizes. The unimodal problems that have only one global minimum whereas for multimodal problems are multiplied local minima's and one global minimum. Unimodal problems help in understanding the exploitative capabilities of an algorithm whereas multi-modal problems are highly challenging problems and help to check both explorative and exploitative tendencies of an algorithm. Thus, the benchmarks will test the effectiveness of the proposed algorithm in terms of explorative and exploitative tendencies. The details of the benchmark functions used is given in Table 1.

In Table 2, the parametric details of the algorithms used for comparison are added. The major algorithm includes SCA [16], WOA [23], SMA [24], EO [25], AO [20], AOA [26], MHA [27], NMRA [28], MFO [29], GWO [30], and MPA [30]. Also, the basic parameters and their corresponding values are presented. Apart from that, the population size 50 and stopping criteria is kept same for all the algorithms. The stopping criteria is the total number of iterations, and in the present case they are equal to1000. For all the algorithms used for comparison, it is kept in mind that the overall number of function evaluations remain same.

5.2. Comparison on classical benchmark problems

The results, which are displayed in Table 3, are meant to assess the performance of the HSCAO algorithm by means of traditional benchmarks. The best, worst, mean, and standard deviation (STD) deviation values of 30 runs are displayed in this table. Other than that, a fixed dimension size of 10 is used to present the findings. Two statistical tests namely Wilcoxon's p-rank and Friedmann tests [32] are done to prove the significance of the proposed algorithm at 5 % level of significance. The results for Wilcoxon's p-rank test are given in terms of win, loss and tie (w/l/t), where w denotes that the suggested algorithm's outcomes are superior to those of the comparator algorithm, whereas l means that the results of the proposed algorithm are worse as compared to the test algorithm and finally t stands for P-tie which indicates that either the outcomes of the two algorithms are statistically similar or there is no correlation between them. The Friedmann test results are presented in the form of a rank commonly referred as f-rank, and the algorithm scoring the best rank is considered as the overall best.

In Tables 3 and Table 4, the comparative results of HSCAO with respect to MSCA, MHA [27], NMRA [28], AO [20], SCA [16], EO [25], MPA [31], WOA [23], GWO [30], and MFO [29] for 10 and 30 dimensional problems respectively. The best, worst, mean, and standard deviation (STD) values of 30 runs are used to display the results. For functions f1 to f4, and f5, f9 to f12, the proposed HSCAO provides the better statistical results whereas for f6 EO provide the best results and for functions f7 and f8 SMA gives the best results. The statistical results in terms of w/l/t and p-test in the last lines of Table 4, shows that of all the algorithms under comparison, the proposed HSCAO scores the first

Table 5
Results of the HSCAO algorithm in compression to other methods for CEC2019 test functions.

Fun No.	Measure	Comparative optimisation algorithms						
		HSCAO	AO	MSCA	SCA	AOA	EO	WOA
$g_1(x)$	**Best**	**3.9418E + 04**	4.4699E + 04	4.1896E + 04	1.4089E + 08	1.3598E + 06	9.8254E + 04	5.8768E + 10
	Worst	4.9605E + 04	9.0952E + 04	9.5831E + 08	3.9500E + 10	3.6414E + 10	5.9835E + 10	1.1350E + 12
	Average	4.2582E + 04	5.4336E + 04	7.5196E + 07	1.1139E + 10	3.4939E + 09	9.0304E + 09	5.6831E + 11
	STD	2.8676E + 03	1.0146E + 04	2.1453E + 08	1.2303E + 10	9.3076E + 09	1.4674E + 10	2.9535E + 11
$g_2(x)$	**Best**	1.7352E + 01	1.7358E + 01	1.7357E + 01	1.7375E + 01	1.8060E + 01	**1.7343E + 01**	4.7742E + 02
	Worst	1.7390E + 01	1.7403E + 01	1.7683E + 01	1.7660E + 01	1.9848E + 01	1.7348E + 01	6.6269E + 03
	Average	1.7369E + 01	1.7377E + 01	1.7391E + 01	1.7467E + 01	1.9217E + 01	1.7345E + 01	2.2372E + 03
	STD	1.0460E-02	1.2255E-02	6.9479E-02	6.2465E-02	5.0702E-01	1.0232E-03	1.8576E + 03
$g_3(x)$	**Best**	**1.2702E + 01**	**1.2702E + 01**	**1.2702E + 01**	**1.2702E + 01**	**1.2702E + 01**	**1.2702E + 01**	**1.2702E + 01**
	Worst	1.2702E + 01	1.2702E + 01	1.2704E + 01	1.2703E + 01	1.2706E + 01	1.2702E + 01	1.2703E + 01
	Average	1.2702E + 01	1.2702E + 01	1.2703E + 01	1.2703E + 01	1.2703E + 01	1.2702E + 01	1.2702E + 01
	STD	7.3412E-06	7.3800E-06	5.3107E-04	9.3470E-05	1.1690E-03	2.2128E-06	3.4768E-05
$g_4(x)$	**Best**	**6.5034E + 01**	1.2634E + 02	2.1982E + 02	6.7852E + 02	6.5138E + 03	9.2181E + 01	2.0577E + 03
	Worst	1.1627E + 03	2.3034E + 03	5.7327E + 03	2.6784E + 03	2.8555E + 04	9.5095E + 02	9.7162E + 03
	Average	1.9799E + 02	8.0077E + 02	1.4759E + 03	1.4844E + 03	1.2325E + 04	4.0440E + 02	5.7255E + 03
	STD	2.3892E + 02	5.4691E + 02	1.8066E + 03	4.9776E + 02	6.1909E + 03	2.2608E + 02	2.2116E + 03
$g_5(x)$	**Best**	1.2456E + 00	1.2655E + 00	1.8299E + 00	2.0374E + 00	2.5903E + 00	**1.1394E + 00**	2.4002E + 00
	Worst	2.0923E + 00	2.2326E + 00	2.4951E + 00	2.3905E + 00	6.0463E + 00	1.7435E + 00	5.1572E + 00
	Average	1.4734E + 00	1.5829E + 00	2.0416E + 00	2.2233E + 00	4.3610E + 00	1.4295E + 00	3.7438E + 00
	STD	2.2704E-01	3.0723E-01	1.6139E-01	9.6322E-02	9.6549E-01	1.6938E-01	8.1991E-01
$g_6(x)$	**Best**	7.9459E + 00	7.9458E + 00	9.6049E + 00	9.8069E + 00	**7.3835E + 00**	9.4559E + 00	8.1841E + 00
	Worst	1.1395E + 01	1.2224E + 01	1.2094E + 01	1.2131E + 01	1.0803E + 01	1.1355E + 01	1.1952E + 01
	Average	1.0172E + 01	1.0755E + 01	1.0950E + 01	1.1110E + 01	8.9877E + 00	1.0136E + 01	1.0727E + 01
	STD	1.0834E + 00	1.0833E + 00	6.5944E-01	6.5974E-01	8.9491E-01	4.2046E-01	9.4789E-01
$g_7(x)$	**Best**	**1.2284E + 01**	8.3454E + 01	3.0144E + 02	4.6046E + 02	3.4101E + 01	1.5945E + 02	6.6138E + 02
	Worst	6.0572E + 02	8.3168E + 02	1.1036E + 03	1.0633E + 03	4.7227E + 02	2.3322E + 02	1.2669E + 03
	Average	2.7575E + 02	3.4378E + 02	7.4648E + 02	8.4291E + 02	2.0528E + 02	1.4805E + 02	9.4509E + 02
	STD	1.5409E + 02	1.8583E + 02	2.1700E + 02	1.6182E + 02	1.2826E + 02	4.5965E + 02	1.7310E + 02
$g_8(x)$	**Best**	**3.5660E + 00**	4.1942E + 00	4.3850E + 00	5.1300E + 00	4.6287E + 00	6.0068E + 00	5.3996E + 00
	Worst	6.5051E + 00	6.0753E + 00	6.8868E + 00	6.8422E + 00	6.1982E + 00	6.9246E + 00	7.3206E + 00
	Average	5.1921E + 00	5.2745E + 00	5.9553E + 00	6.1248E + 00	5.5875E + 00	6.3167E + 00	6.4517E + 00
	STD	7.9635E-01	5.7805E-01	6.0817E-01	5.0553E-01	4.8782E-01	2.5292E-01	4.8119E-01
$g_9(x)$	**Best**	**2.7606E + 00**	2.9956E + 00	4.6422E + 00	2.2902E + 01	2.7924E + 02	2.7933E + 00	4.8685E + 02
	Worst	6.1373E + 00	6.4775E + 00	2.9170E + 02	2.6481E + 02	1.6400E + 03	5.6484E + 00	1.2954E + 03
	Average	4.4169E + 00	5.0082E + 00	3.5617E + 01	1.0021E + 02	7.5734E + 02	4.0023E + 00	8.4974E + 02
	STD	1.0163E + 00	1.0171E + 00	8.5592E + 01	5.9906E + 01	3.8309E + 02	9.3267E-01	2.4361E + 02
$g_{10}(x)$	**Best**	**2.9159E + 00**	3.3682E + 00	2.0368E + 01	2.0329E + 01	2.0003E + 01	2.0418E + 01	2.0143E + 01
	Worst	2.0619E + 01	2.0562E + 01	2.0647E + 01	2.0558E + 01	2.0410E + 01	2.0663E + 01	2.0621E + 01
	Average	1.8012E + 01	1.9173E + 01	2.0513E + 01	2.0464E + 01	2.0204E + 01	2.0555E + 01	2.0397E + 01
	STD	5.8520E + 00	4.0794E + 00	7.5293E-02	6.7826E-02	1.2243E-01	7.4320E-02	1.2563E-01
(W|L|T)		(6|3|1)	(0|9|1)	(0|9|1)	(0|9|1)	(1|8|1)	(2|7|1)	(0|9|1)
Mean		1.7	2.9	4.1	5.3	4.5	3.7	5.8
Ranking		1	2	4	6	5	3	7

rank. Apart from that the convergence patterns shown in the Fig. 5, shows that the proposed HSCAO converges significantly faster for most of the test problems with respect to other algorithms. In addition, it was the most competitive processing time when it is compared with the other relative optimization algorithms. Hence, it was the most robust and efficient to rest at solving issues by the population size. Consequently, it is carried to implement in the real application test of power system network that requires the higher processing time to address the high fluctuations in frequency response.

5.3. CEC 2019 benchmark results

In this subsection, extensive results on CEC-2019 benchmarks are presented in Table 5. The CEC 2019 benchmark suite is a 100-digit problem test suite and consists of 10 highly challenging problems [33]. The same set of algorithms namely MSCA, AO [20], SCA [16], AOA [26], EO [25], and WOA [23], are used for a comparative study with respect to HSCAO. The results are presented as the best, worst, mean and STD values of 30 runs. The results in Table 5 shows the HSCAO was achieving the best performs for the function g1, g3, g4, g7 to g10, in contract, the EO gives the best results at function g2 and g5. Overall, the proposed HSCAO was the best for eight benchmark problems across the iterations number, while EO algorithm was the good performance at two problems only. Meanwhile, other comparative algorithms delis to address the local solutions. This can be further acknowledged from the convergence curves in Fig. 6 when it is addressing the processing time of the issues compared with the relative optimization algorithms. From the convergence curves, we can see that the HSCAO algorithm has the best convergence patterns with respect to other algorithm for most of the test functions. As results, this further proves that the HSCAO performs significantly better for these problems and can be considered as a potential candidate for future optimization research. Hence, the proposed algorithm is implemented within the PID-AGC system to addressing the sensitivity of power system network by addressing the uncertain parameters of the controller due to its fastest processing time when it is compared with other relative optimization algorithm tests.

5.4. Optimisation problem

Following the validation of the HSCAO algorithm using the classical and CEC-2019 benchmark issues, which demonstrate the wide-ranging performance of the suggested algorithm in comparison to the relative optimization algorithms, Fig. 7 illustrates the use of the suggested PID control in conjunction with an AGC for a two-area power system. On the basis of the validation tests, Table 6 presents the main parameters of the HSCAO algorithm. Table 7's parameters are then used to apply this hybrid HSCAO algorithm to the two-area power grid. The historical changing error of the frequency response and power generation of the

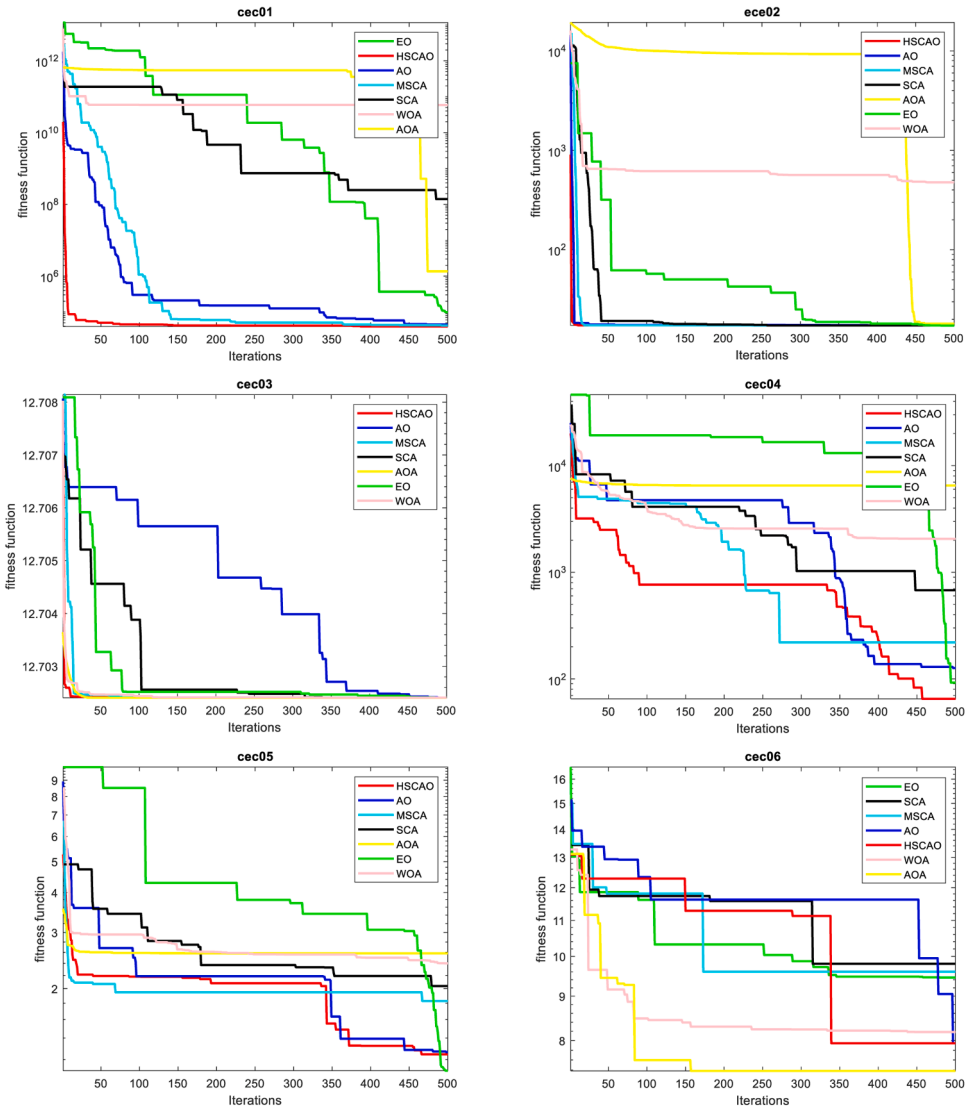

Fig. 6. Convergence curves for different algorithm based on CEC-2019 benchmarks.

application test are employed as the input signal of the robust PID-AGC, whilst, the signal of the governor is addressed as the output, as discussed in Eq. (36) and Eq. (37). Hence, The HSCAO algorithm addresses the accurate parameters of the robust PID-AGC with the minimum ITAE performance index as expressed in following Eq. (54) [34]:

$$\mathrm{ITAE} = \int_0^t \left(/\Delta \mathrm{F_i}\right/ + \left/\Delta P_{tie}\right/ .t\ dt \tag{54}$$

This objective function based on ITAE index is used to minimize the overshoot and oscillations of the frequency response and the power delivery of the power system based on the optimal control theory. Consequently, the optimal parameters of the PID control are addressing to design the robust AGC system for the multi-area power system network, as presented in Table 8. This is because the optimal state feedback control based on hybrid algorithm such as HSCAO algorithm gives the better behavior systematic tuning trade-offs between the tracking signal of the power disturbances and the control activity of frequency response. As a result, it will address the challenges of the computational complexity and feasibility of power system networks [35, 36]. In the next step, this robust PID-AGC system based on the HSCAO algorithm is addressed the parameters of PID control and AGC system under various scenarios when it is applied on the two-area power system network to show the stability and scalability of its performance. This proposed algorithm has a faster processing time to find the parameters as explained in section 4 and proved in section 5.

6. Results and discussion

A MATLAB Simulink model environment for a two-area power network is designed to test the robust PID-AGC system. Next, it is distinguished with the FLC-AGC, and PID-AGC to demonstrate its efficacy and scalability. Then, the ITAE performance index is employed to determine the transient response time of the system under three disturbance cases. After that, the three simulation scenario cases are considered as following: simple step changing load-disturbance, variable step changing load-disturbance and unbalance step changing load-disturbance. Those disturbance tests are represented various cases that occurs in a competitive load-demand to test the high sensitivity of AGC. Finally, they are employed for the two-area power network to analysis the sensitivity of the robust PID-AGC control for each area.

In the first case, the simple step-load disturbances are simulated based on the rapid changing from 0 % to 60 % at 50 seconds and unchanging for area-1 and area-2, respectively. Although, both of the

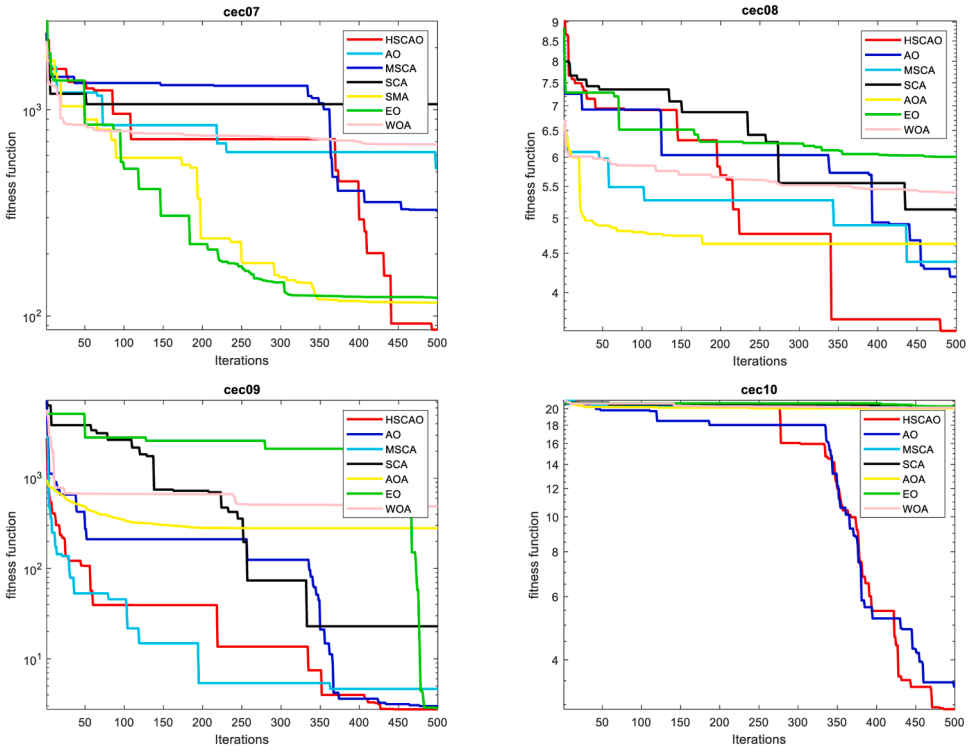

Fig. 6. (*continued*).

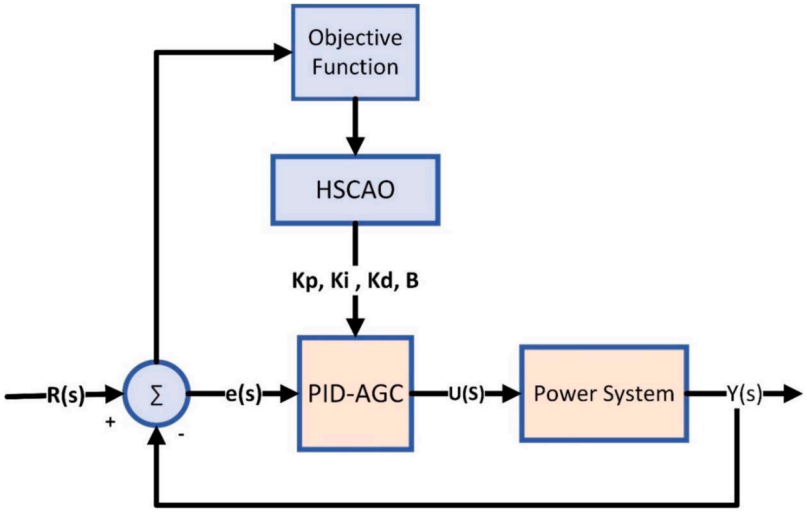

Fig. 7. The block diagram of PID-AGC based on the HSCAO algorithm.

Table 6
The fitting parameters of HSCAO algorithm.

Parameters	Value
Alpha	0.1
Delta	0.1
Omega	0.005
Beta	1.5
Dimension of search space	100
Population size	50
Standard deviation	30
Linear reduction	2
Search cycles ranging	1-20

Table 7
The designed parameters of power system based on area.

Parameters	Area 1	Area 2
The power generation unit (MW)	250	400
The frequency level (Hz)	50	50
The speed governor (pu)	0.05	0.0625
The time governor (sec.)	0.2 sec	0.3 sec
The time turbine (sec.)	0.5 sec	0.6 sec
The inertia generator (sec.)	5	4
The sensitivity of load-coefficient	0.6	0.9

Table 8
The tuning parameters of Optimal PID-AGC vs Conventional PID-AGC.

The area of power system	Conventional PID-AGC	Robust PID-AGC
Area-1	B1= 20	B1=20
	Kp= 0.7	Kp= 58.55
	Ki= 2	Ki= 98.45
	Kd= 1	Kd= 39.57
Area-2	B= 16.92	B=16.92
	Kp= 0.7	Kp= 78.54
	Ki= 2	Ki= 99.72
	Kd= 1	Kd= 59.78

robust controller and classical controllers were an independent frequency response for this simple load fluctuations, as presented in Fig. 8 (a) and (b). However, the AGC system of the optimised PID controller was the most reliable to response the deviation loads of costumer tests when compared to the FLC-AGC and PID-AGC that have been fluctuating around the reference test signal with higher overshoots. Furthermore, the power deliveries of the generation units were the highest stability with the lowest steady state error comparison to the same approaches as well as it was the lest overshoot, as shown in Fig. 8(b) and (c). In contrast, the conventional FLC-AGC and PID-AGC are taking a bite longer time to address the reference value of the frequency response with the higher maximum rise time for various changing steps compared to the proposed method. As results, it is achieved the lowest ITAE index about 0.6s whiles the conventional FLC-AGC and PID-AGC were about 2.7s and 3.9s.

In the second case, the complex step-load disturbances are employed on the area-1 changing as following; 40 %, 80 %, 40 % and 20 % at 10 seconds,0 second, 30 seconds and 40 seconds respectively. While, the step- load disturbance of the area-2 is changing from 0 %, 40 %, 10 %, 40 % and 20 % at 10 second, 30 seconds and 40 seconds. The outcome of this test shows that the robust PID controller is also achieved the highest stability for frequency response with the lowest fluctuation around the standard frequency response of the power grid when it is applied on those variable load disturbances regarding to the comparison controller cases, as presented in Fig. 9(a) and (b). Further, the power generation of both areas are confirmed the enhancement in the performance according to its minimizing convergence time with the lowest oscillation compared with the other approach controllers, as explained in Fig. 9(c) and (d). In other side, the conventional PID-AGC and conventional FLC-AGC were a lesser dynamic performance to address the overshoot and the oscillation at various time tests. Moreover, they tack a bite longer time to much the power demand with power generation. Hence, the robust PID-AGC is approved the best validation test when it reaches to the stability state at ITAE index of 3.9s while the conventional FLC-AGC and PID-AGC are 8.7s and 14.5s respectively.

Lastly, the third scenario is designed based on an unbalance load-disturbance to assess the validation of the proposed PID approach under a fault-case. This unbalance condition-test is rapidly changing for simulation signal that is value of 0.25pu-amplitude and 50 Hz-frequency scale for a sinusoidal wave. As noticed in Fig. 10, the three-controller systems face a huge fluctuation challenge around the standard frequency level at various simulation time. However, the proposed controller was the least steady-state error of oscillation response for the frequency level and power delivery of the grid-connected regrading to the FLC-AGC and PID-AGC. In addition, it was the most damping ratio to address the zero-point state with the lowest overshoot and rising time during all the time test comparison with the other classical approaches. Further, it was the lowest oscillation for the frequency response and power delivery at the various states. Hence, it achieves the acceptable fluctuating frequency response regarding to the standard value which is less than ± 0.5 % during the test time. Consequently, it is achieved the best ITAE performance index about 5.2s compared to the FLC-AGC and PID-AGC of 10.9s and 17.4s respectively. This is because the optimal PID-AGC based on the HSCAO algorithm gives the highest robust trade-offs between disturbances and the wide variation of PID-AGC parameters. In other side, the conventional PID-AGC was the faster to address the steady state error compared with the FLC-AGC system. Finally, the summarizing results of ITAE index of these three scenarios are depicted in Table 9. Whilst, the sensitivity of AGC system using the five seconds of interval Simulink time at the fault condition is presented in Table 10,

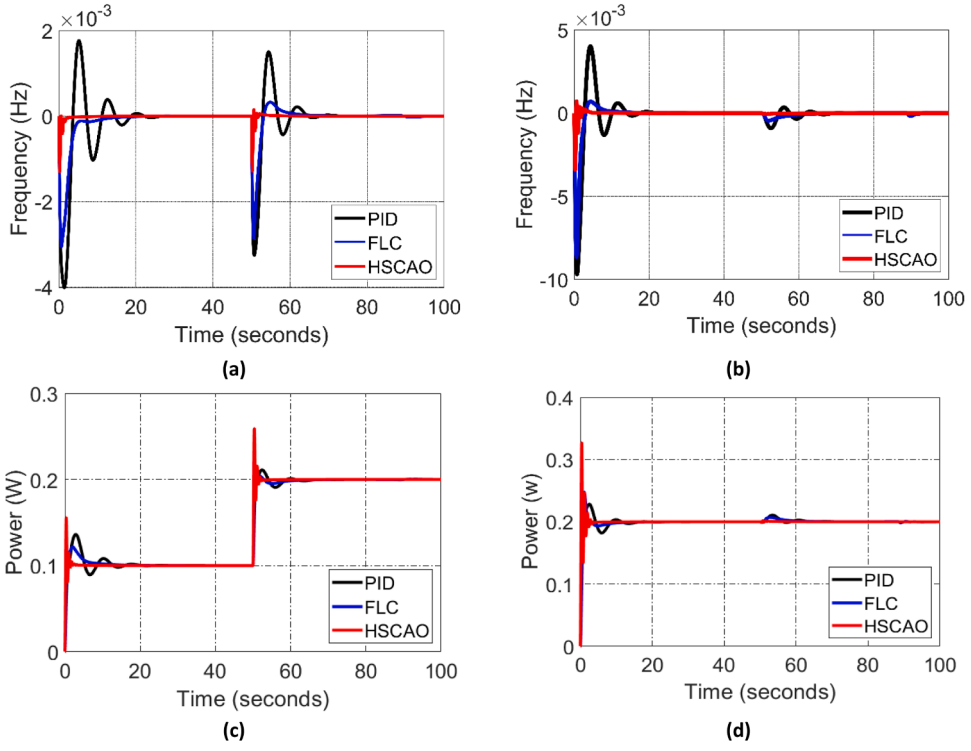

Fig. 8. The outcome of case-1 for (a)frequency of area-1, (b)frequency of area-2, (c)power of area-1and (c)power of area-2.

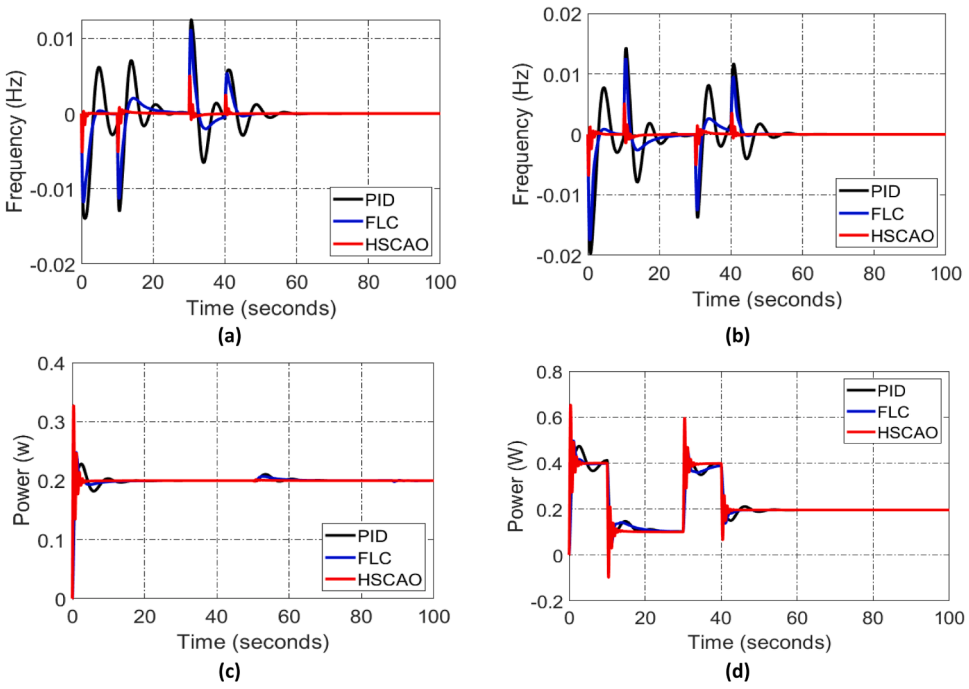

Fig. 9. The results of case-2 for (a)frequency of area-1, (b)frequency of area-2, (c)power of area-1and (c)power of area-2.

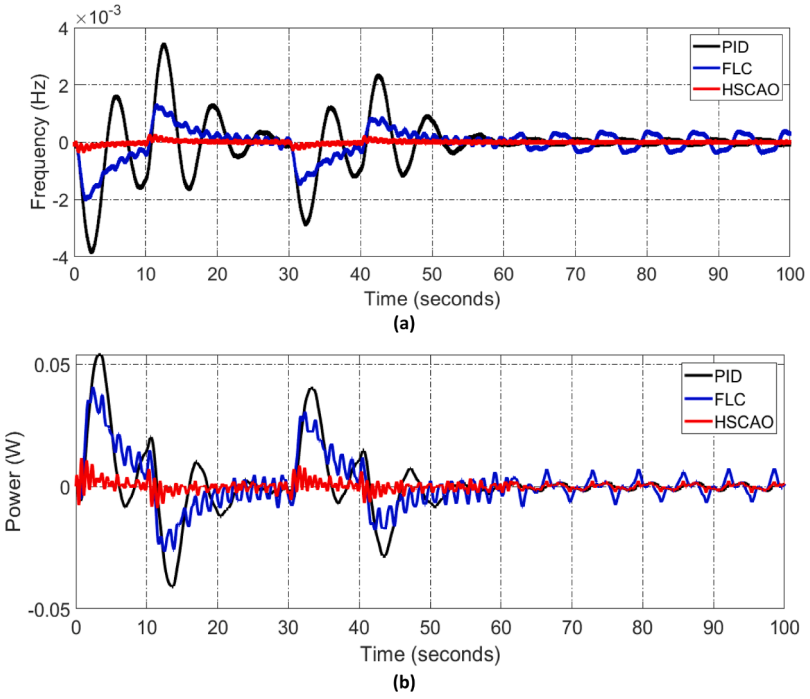

Fig. 10. (a) Oscillation response in frequency and (b) Output-Power delivery, at an unbalance power disturbance (case-3).

Table 9
The total ITAE value for Proposed method, FLC method and PID method.

Method	ITAE performance index		
	Case-1	Case-2	Case-3
Robust PID-AGC	0.6	3.9	5.2
Conventional FLC-AGC	2.7	8.7	10.9
Conventional PID-AGC	3.9	14.5	17.4

which shows the robustness of proposed PID method based on the HSCAO algorithm when compared with the conventional FLC controller and the conventional PID controller which shows that the proposed algorithm addresses the parameters of PID-AGC adequately, resulting in, achieving the lower ITAE index in various time intervals.

7. Conclusions

The robust PID controller for the higher performance AGC in a two-area power system network has been designed in this study using the

Table 10
The sensitivity of AGC system based on interval time.

Time	Δf1			Δf2			ΔP-tie line			ITAE		
	Robust PID	FLC	PID	Robust PID	FLC	PID	Robust PID	FLC	PID	Robust PID	FLC	PID
0	0	0	0	0	0	0	0	0	0	0	0	0
5	−0.0001	0.0009	−0.0009	0.0001	0.0066	0.0018	0.0016	0.0078	0.0206	0.0523	0.2115	0.5004
10	0.0009	−0.026	−0.0048	0.0011	0.0085	0.0149	0.0062	0.0941	0.0667	0.1554	1.9506	2.5708
15	0.0005	−0.0008	0.0007	−0.0001	−0.0053	−0.0012	−0.001	−0.0026	−0.0133	0.5834	2.1383	4.2128
20	0.0006	0.0013	0.0004	−0.0001	−0.0005	−0.0003	−0.0004	−0.0063	−0.0041	0.5891	3.758	4.3523
25	0.0001	0.0002	0.0002	−0.0001	0.0003	−0.0001	−0.0002	−0.0021	−0.0015	0.599	4.6042	4.3593
30	0.0002	−0.0001	0.0002	−0.0001	−0.0001	−0.0001	−0.0001	−0.0004	−0.0004	0.5918	5.013	4.3651
35	0.0091	0.0408	−0.1006	0.0801	0.1049	0.2014	0.0112	0.2056	0.6153	3.0953	6.8698	14.5378
40	0.0051	−0.0016	−0.0003	0.0001	0.0066	0.0083	0.0056	0.0069	0.0049	3.1084	9.7653	14.8569
45	0.0042	−0.0085	0.0084	−0.0071	−0.0036	−0.0098	−0.0017	−0.0036	−0.0188	3.4643	12.617	20.9939
50	0.0001	0.0009	0.0002	−0.0001	−0.0003	−0.0002	−0.0003	−0.0042	−0.0028	3.4757	15.7262	21.2676
55	0.0001	0.0001	0.0002	−0.0001	0.0002	−0.0001	−0.0001	−0.0014	−0.0011	3.4775	16.1139	20.2815
60	0.0001	0.0001	0.0002	−0.0001	−0.0001	−0.0001	−0.0001	−0.0036	−0.0004	3.4804	15.7455	20.2993
65	0.0001	0.0001	−0.0001	−0.0001	0.0001	−0.0001	−0.0001	−0.0001	−0.0008	3.4829	18.189	20.3166
70	0.0001	0.0002	−0.0003	0.0001	0.0001	−0.0001	0.0001	0.0011	0.0001	3.4837	18.6858	20.3604
75	0.0051	0.0012	0.0012	−0.0011	−0.0021	0.0091	−0.0011	−0.0082	0.0018	4.4844	19.1997	20.4334
80	0.0041	0.0001	0.0004	−0.0081	−0.0011	0.0041	−0.0091	−0.0082	0.0003	4.4855	19.7782	20.4956
85	0.0021	−0.0001	0.0002	−0.0001	0.0001	−0.0001	−0.0001	0.00013	−0.0007	4.4863	20.3594	20.573
90	0.0051	0.0082	−0.0102	0.0061	0.0091	−0.0401	0.0091	0.02028	−0.0904	5.4873	21.0226	21.6491
95	0.0001	0.0002	−0.0003	0.0001	−0.0001	0.0001	0.0001	0.0001	0.0005	5.4883	21.6785	22.7289
100	0	0	0	0	0	0	0	0	0	0	0	0

HSCAO algorithm. Firstly, the HSCAO optimisation tools have been implemented to address the main elements of the PID-AGC controller. Next, it is assessed on CEC-2019 and classical benchmark issues with different dimensions to set the better parameter fits of the proposed algorithm. Also, statistical analysis techniques based on Wilcoxon's test and Friedman' test have been applied to prove the outstanding interpretation of this HSCAO algorithm compared with other optimsation algorithms. Then, ITAE index is used as fitness function to determine the transiting time of the frequency response. Finally, it is employed on the real time application of the power system network, after addressing the main parameters of PID-AGC system that is built based on MATLAB environment regarding to the state space model. The finding results demonstrate that the proposed method iterates the value of frequency operation to standard value of power system in less time and improves the power delivery of the multi-area test compared with the conventional FLC and PID methods with addressing the fault condition test under several states. Consequently, it achieves the lowest ITAE indexes about 0.6s, 3.9s and 5.2s for the simple disturbance, and complex disturbance and fault disturbance, respectively. Whilst, the FLC-AGC and PID-AGC controllers accomplishes to 2.7s, 8.7s and10.9s and 3.9s, 14.5s and 17.4s respectively. In future work, it will be used to dampen the oscillation level in frequency response of a hybrid power system network under double fault tests.

CRediT authorship contribution statement

Sadeq D. Al-Majidi: Methodology, Conceptualization. **Al_hussein M. Alturfi:** Data curation. **Mohammed Kh. Al-Nussairi:** Formal analysis. **Rasha Abed Hussein:** Writing – review & editing. **Rohit Salgotra:** Data curation. **Maysam F. Abbod:** Methodology.

Declaration of competing interest

I am writing to confirm to you that there are no conflicts of interest

Data availability

Data will be made available on request.

References

[1] R. Verma, S.K. Gawre, N.P. Patidar, S. Nandanwar, A state of art review on the opportunities in automatic generation control of hybrid power system, Electric Power Syst. Res. 226 (2024), https://doi.org/10.1016/j.epsr.2023.109945.

[2] S.D. Al-Majidi, H.D.S. Altai, M.H. Lazim, M.K. Al-Nussairi, M.F. Abbod, H.S. Al-Raweshidy, Bacterial foraging algorithm for a neural network learning improvement in an automatic generation controller, Energies (Basel) 16 (6) (2023), https://doi.org/10.3390/en16062802.

[3] G. Ahmed, A. Eltayeb, N.M. Alyazidi, et al., Improved particle swarm optimization for fractional order PID control design in robotic manipulator system: a performance analysis, Results Eng. 24 (2024) 103089, https://doi.org/10.1016/j.rineng.2024.103089.

[4] Y. Arya, AGC of two-area electric power systems using optimized fuzzy PID with filter plus double integral controller, J. Franklin Inst. 355 (11) (2018) 4583–4617, https://doi.org/10.1016/j.jfranklin.2018.05.001.

[5] Y. Arya, Improvement in automatic generation control of two-area electric power systems via a new fuzzy aided optimal PIDN-FOI controller, ISA Trans. 80 (2018) 475–490, https://doi.org/10.1016/j.isatra.2018.07.028.

[6] J.R. Nayak, B. Shaw, B.K. Sahu, Application of adaptive-SOS (ASOS) algorithm-based interval type-2 fuzzy-PID controller with derivative filter for automatic generation control of an interconnected power system, Eng. Sci. Technol., Int. J. 21 (3) (2018) 465–485, https://doi.org/10.1016/j.jestch.2018.03.010.

[7] J.R. Nayak, B. Shaw, B.K. Sahu, K.A. Naidu, Application of optimized adaptive crow search algorithm based two degrees of freedom optimal fuzzy PID controller for AGC system, Eng. Sci. Technol., Int. J. 32 (2022), https://doi.org/10.1016/j.jestch.2021.09.007.

[8] B.P. Sahoo, S. Panda, Improved grey wolf optimization technique for fuzzy aided PID controller design for power system frequency control, Sustain. Energy, Grids and Networks 16 (2018) 278–299, https://doi.org/10.1016/j.segan.2018.09.006.

[9] N.E.Y. Kouba, M. Menaa, M. Hasni, M. Boudour, A novel optimal combined fuzzy PID controller employing dragonfly algorithm for solving automatic generation control problem, Electric Power Comp. Syst. 46 (19–20) (2018) 2054–2070, https://doi.org/10.1080/15325008.2018.1533604.

[10] N. Nayak, S. Mishra, D. Sharma, B.K. Sahu, Application of modified sine cosine algorithm to optimally design PID/fuzzy-PID controllers to deal with AGC issues in deregulated power system, IET Gener. Transm. Distrib. 13 (12) (2019) 2474–2487, https://doi.org/10.1049/iet-gtd.2018.6489.

[11] P.C. Sahu, R. Baliarsingh, R.C. Prusty, S. Panda, Automatic generation control of diverse energy source-based multiarea power system under deep Q-network-based fuzzy-T2 controller, Energy Sources, Part A: Recovery, Utilization and Environ. Effects (2020), https://doi.org/10.1080/15567036.2020.1809568.

[12] A. Daraz, et al., Automatic generation control of multi-source interconnected power system using FOI-TD controller, Energies (Basel) 14 (18) (2021) 5867, https://doi.org/10.3390/en14185867.

[13] N. Kumari, P. Aryan, G.L. Raja, Y. Arya, Dual degree branched type-2 fuzzy controller optimized with a hybrid algorithm for frequency regulation in a triple-area power system integrated with renewable sources, Protection and Control of Modern Power Syst. 8 (1) (2023), https://doi.org/10.1186/s41601-023-00317-7.

[14] D.K. Gupta, et al., Fractional order PID controller for load frequency control in a deregulated hybrid power system using Aquila Optimization, Results in Eng. 23 (2024) 102442, https://doi.org/10.1016/j.rineng.2024.102442.

[15] M.K. Debnath, R. Agrawal, S.R. Tripathy, S. Choudhury, Artificial neural network tuned PID controller for LFC investigation including distributed generation, Int. J.

Numer. Model. Electron. Networks, Devices Fields 33 (5) (2020) 1–17, https://doi.org/10.1002/jnm.2740.
[16] K.H. Almotairi, L. Abualigah, Hybrid reptile search algorithm and remora optimization algorithm for optimization tasks and data clustering, Symmetry (Basel) 14 (3) (2022), https://doi.org/10.3390/sym14030458.
[17] S.Goyal Al hussein M. Alturfi, A. Kaur, The optimum design of scanned linear antenna array using sine cosine optimization algorithm, Wasit J. Comput. Math. Sci. 2 (2) (2023), https://doi.org/10.31185/wjcms.135.
[18] S. Gupta, K. Deep, A hybrid self-adaptive sine cosine algorithm with opposition-based learning, Expert Syst. Appl. 119 (2019) 210–230, https://doi.org/10.1016/j.eswa.2018.10.050.
[19] H. Nenavath, D.R. Kumar Jatoth, D.S. Das, A synergy of the sine-cosine algorithm and particle swarm optimizer for improved global optimization and object tracking, Swarm Evol. Comput. 43 (2018) 1–30, https://doi.org/10.1016/j.swevo.2018.02.011.
[20] L. Abualigah, D. Yousri, M. Abd Elaziz, A.A. Ewees, M.A.A. Al-qaness, A. H. Gandomi, Aquila Optimizer: a novel meta-heuristic optimization algorithm, Comput. Ind. Eng. 157 (2021), https://doi.org/10.1016/j.cie.2021.107250.
[21] S. Wang, H. Jia, Q. Liu, R. Zheng, An improved hybrid aquila optimizer and harris hawks optimization for global optimization, Math. Biosci. Eng. 18 (6) (2021), https://doi.org/10.3934/mbe.2021352.
[22] H. Liu, X. Zhang, H. Zhang, C. Li, Z. Chen, A reinforcement learning-based hybrid aquila optimizer and improved arithmetic optimization algorithm for global optimization, Expert Syst. Appl. 224 (2023), https://doi.org/10.1016/j.eswa.2023.119898.
[23] S. Mirjalili, A. Lewis, The whale optimization algorithm, Adv. Eng. Software 95 (2016), https://doi.org/10.1016/j.advengsoft.2016.01.008.
[24] S. Li, H. Chen, M. Wang, A.A. Heidari, S. Mirjalili, Slime mould algorithm: a new method for stochastic optimization, Future Generat. Comput. Syst. 111 (2020), https://doi.org/10.1016/j.future.2020.03.055.
[25] A. Faramarzi, M. Heidarinejad, B. Stephens, S. Mirjalili, Equilibrium optimizer: a novel optimization algorithm, Knowl. Based. Syst. 191 (2020), https://doi.org/10.1016/j.knosys.2019.105190.
[26] L. Abualigah, A. Diabat, S. Mirjalili, M.Abd Elaziz, A.H. Gandomi, The arithmetic optimization algorithm, Comput. Methods Appl. Mech. Eng. 376 (2021), https://doi.org/10.1016/j.cma.2020.113609.
[27] R. Salgotra, U. Singh, S. Singh, N. Mittal, A hybridized multi-algorithm strategy for engineering optimization problems, Knowl. Based. Syst. 217 (2021), https://doi.org/10.1016/j.knosys.2021.106790.
[28] R. Salgotra, U. Singh, The naked mole-rat algorithm, Neural. Comput. Appl. 31 (12) (2019), https://doi.org/10.1007/s00521-019-04464-7.
[29] S. Mirjalili, Moth-flame optimization algorithm: a novel nature-inspired heuristic paradigm, Knowl. Based. Syst. 89 (2015), https://doi.org/10.1016/j.knosys.2015.07.006.
[30] S. Mirjalili, S.M. Mirjalili, A. Lewis, Grey wolf optimizer, Adv. Eng. Software 69 (2014), https://doi.org/10.1016/j.advengsoft.2013.12.007.
[31] A. Faramarzi, M. Heidarinejad, S. Mirjalili, A.H. Gandomi, Marine predators algorithm: a nature-inspired metaheuristic, Expert Syst. Appl. 152 (2020), https://doi.org/10.1016/j.eswa.2020.113377.
[32] J. Derrac, S. García, D. Molina, F. Herrera, A practical tutorial on the use of nonparametric statistical tests as a methodology for comparing evolutionary and swarm intelligence algorithms, Swarm. Evol. Comput. 1 (1) (2011) 3–18, https://doi.org/10.1016/j.swevo.2011.02.002.
[33] K. V Price, N. H. Awad, M. Z. Ali, and P. N. Suganthan, "The 100-Digit Challenge: Problem Definitions and Evaluation Criteria for the 100-Digit Challenge Special Session and Competition on Single Objective Numerical Optimization," 2018. [Online]. Available: http://www.ntu.edu.sg/home/EPNSugan/index_files/CEC2019.
[34] M. Zaidi Mohd Tumari, M. Ashraf Ahmad, M. Ikram Mohd Rashid, A fractional order PID tuning tool for automatic voltage regulator using marine predators algorithm, Energy Reports 9 (2023) 416–421, https://doi.org/10.1016/j.egyr.2023.10.044.
[35] L.P. Qian, S. Han, B. Ji, Y. Zhang, Editorial: machine learning and intelligent communications (MLICOM 2018), Mob. Networks Appl. 27 (3) (2022) 1081–1083, https://doi.org/10.1007/s11036-022-01979-7.
[36] S.M. Radhi, S.D. Al-Majidi, M.F. Abbod, H.S. Al-Raweshidy, Machine learning approaches for short-term photovoltaic power forecasting, Energies 17 (17) (2024) 1–23, https://doi.org/10.3390/en17174301.